



A Red Giants' Toy Story

Marcelo M. Miller Bertolami^{1,2} ¹ Instituto de Astrofísica de La Plata, Consejo Nacional de Investigaciones Científicas y Técnicas Avenida Centenario (Paseo del Bosque) S/N, B1900FWA La Plata, Argentina; mmiller@fcaglp.unlp.edu.ar² Facultad de Ciencias Astronómicas y Geofísicas, Universidad Nacional de La Plata Avenida Centenario (Paseo del Bosque) S/N, B1900FWA La Plata, Argentina marcelo@mpa-garching.mpg.de*Received 2022 February 11; revised 2022 August 26; accepted 2022 October 6; published 2022 December 19*

Abstract

In spite of the spectacular progress accomplished by stellar evolution theory, some simple questions remain unanswered. One of these questions is “Why do stars become red giants?”. Here we present a relatively simple analytical answer to this question. We validate our analysis by constructing a quantitative toy model of a red giant and comparing its predictions to full stellar evolutionary models. We find that the envelope forces the value of $\nabla = d \ln T / d \ln P$ at, and above, the burning shell into a very narrow range of possible values. Together with the fact that the stellar material at the burning shell both provides and transports most of the stellar luminosity, this leads to tight relations between the thermodynamic variables at the burning shell and the mass and radius of the core— $T_s(M_c, R_s)$, $P_s(M_c, R_s)$, and $\rho_s(M_c, R_s)$. When complemented by typical mass–radius relations of the helium cores, this implies that for all stellar masses the evolution of the core dictates the values of T_s , P_s , and ρ_s . We show that for all stellar masses evolution leads to an increase in the pressure and density contrasts between the shell and the core, forcing a huge expansion of the layers on top of the burning shell. Besides explaining why stars become red giants our analysis also offers a mathematical demonstration of the so-called shell homology relations, and provides simple quantitative answers to some properties of low-mass red giants.

Unified Astronomy Thesaurus concepts: [Stellar structures \(1631\)](#); [Red giant stars \(1372\)](#); [Stellar interiors \(1606\)](#); [Giant branch \(650\)](#)

1. Introduction

About a century from its humble beginnings (Eddington 1926), stellar evolution theory has developed into a full-fledged predictive theory (Kippenhahn et al. 2012) whose results are routinely used as inputs for other fields of astrophysics (Greggio & Renzini 2011; Cassisi & Salaris 2013). Its predictions have been confirmed by a variety of different observational tests, and are continuously checked by countless numerical simulations by means of specifically tailored numerical codes (Lebreton et al. 2008; Silva Aguirre et al. 2020). In spite of the spectacular progress accomplished, some simple questions remain unanswered. One of these questions is “Why do stars become red giants?”. Although the existence of a red giant solution is known since the early days of automatic numerical computations (Öpik 1938; Hayashi 1947, 1949; Hoyle & Schwarzschild 1955), no simple explanation of the reason for the existence of such a solution has been provided. The absence of a universally accepted answer for this question can be clearly appreciated by reading the related chapters in textbooks of stellar evolution. When trying to explain the evolution after the end of core-hydrogen (H) burning, different authors choose very different paths. Some authors choose to describe extensively the details of numerical models (Iben 2013), others choose to establish an ad hoc principle that applies exclusively to stellar evolution (e.g., the so-called “mirror principle of radial motions”; Kippenhahn et al. 2012), others try to convince themselves that not all physical processes can be understood in simple step-by-step terms and that we should accept the raw output of numerical

simulations (Prialnik 2009), while others openly admit that we lack a definitive explanation of the precise physical reason(s) that drive the expansion (Hansen et al. 2004; Salaris & Cassisi 2005).

The lack of an accepted answer does not mean that no answers have been proposed but just that proposed answers have never attained wide popularity. And for good reasons. Proposed answers encompass a wide variety of ideas, too vast and complex for this introduction. With no intention of being exhaustive, but to highlight both the complexity of the problem and its many possible angles, let us mention a few of them. As mentioned by Eggleton & Faulkner (1981), one of the most ubiquitous myths among nonspecialists is the idea that the gravitational energy released by the contracting core is absorbed by the envelope causing it to expand, ignoring the fact that most of the energy comes from the burning shell and the envelope has no way to tell where the energy is coming from. Similarly ubiquitous is the statement that the increase in the stellar radius is a consequence of the increase in the energy output of the burning shell due to the heating of the core, also ignoring the fact that in low-mass stars the core is mostly heated by the surrounding envelope (and not the other way around), and that there is no obvious reason why the burning shell would not settle at a lower temperature, which would imply a huge decrease in the energy output of the burning shell. While it might be expected that nonspecialists find it hard to pin down the reasons why stars become red giants, it is much more interesting that experts in stellar structure have also failed to agree on the actual causes of this transformation. While studying this problem some authors have highlighted the importance of the gravitational field generated by the compact core by numerically solving steady-state solutions (*thermal equilibrium*, $dS/dt = 0$; Höppner & Weigert 1973; Eggleton & Faulkner 1981; Weiss 1983). Others have focused on the chemical gradients developed due to nuclear reactions at the

burning shell (Hoyle & Lyttleton 1949). Some authors have highlighted the key importance of the degree of central condensation of the core and its consequences on the envelope (Eggleton & Cannon 1991; Faulkner 2005). While all the works mentioned before have been focused on the study of the consequences of different core properties in steady-state solutions, some other authors have concluded that giantness is a consequence of thermal instabilities in the envelope due to the high luminosity released by the burning shell (Renzini 1984; Applegate 1988; Renzini et al. 1992; Renzini & Ritossa 1994). Also in this connection, some authors have pointed to the development of some gravothermal catastrophe of the core and the entropy gradient above it (Fujimoto & Iben 1991). The methods adopted to try to answer this question have also been extremely diverse. For example, some authors have tried to answer the question by constructing simplified ad hoc polytropic models (Eggleton & Cannon 1991; Frost & Lattanzio 1992; Eggleton et al. 1998), some have tried to answer this question by means of dimensional analysis (Bhaskar & Nigam 1991), while others have tried to answer the question by a detailed evaluation of numerical solutions on the U - V plane (Fujimoto & Iben 1991; Sugimoto & Fujimoto 2000). While some authors have highlighted the importance of some critical curves and singular points in the U - V plane (Yahil & van den Horn 1985; Sugimoto & Fujimoto 2000), others have disparaged these explanations as mere descriptions of the results from numerical models (Iben 1993). Proposed answers also encompass a wide diversity in complexity, from very simple (Hauptmann et al. 2000) to extremely complex (Whitworth 1989). The discussions about why stars become red giants have sometimes turned into heated debates (Sugimoto 1997; Faulkner 1997; Sugimoto & Fujimoto 2000; Faulkner 2005), while some other times authors have ignored criticism and continue to develop ideas (Renzini et al. 1992; Renzini & Ritossa 1994) that had already been seriously questioned by other researchers (Weiss 1989; Iben 1993). The reader interested in the subtleties and shortcomings of the different ideas is referred to the appendix of Sugimoto & Fujimoto (2000), Appendix 10.B of Faulkner (2005), the introductions to Applegate (1988) and Stancliffe et al. (2009), and Section 3.3 of Bhaskar & Nigam (1991).

Both Whitworth (1989) and Iben (1993) concluded that a simple explanation of why stars become red giants is not possible. Iben (1993) issued a warning against attempts to find simple explanations, claiming that simple explanations might be forcefully misleading. Although we are aware of these warnings, this paper is an attempt to shed some light on a possible simple explanation on the question of why do stars become red giants. We understand this to be a worthwhile project because toy models and dimensional analysis play a key role in how our minds approach the understanding of physical problems. We believe that toy models are key to extrapolate the results of a set of numerical simulations to all *similar* stars and to other *analogous* physical problems. In fact, in order to define what the words *similar* and *analogous* in the previous sentence mean, a toy-model description of the problem is a necessity. For this reason we have searched for a toy-model description of red giants that is both accurate and convincing. In constructing our toy model we have kept in mind the warnings by Iben (1993) regarding “convoluted arguments” and “circular explanations”. We have forced ourselves to avoid the use of particular properties

observed in detailed stellar models in the construction of our toy model, and kept the line of reasoning as clear as possible.

In our opinion, numerical experiments with steady-state solutions (thermal equilibrium) like those performed by Hoppner & Weigert (1973), Weiss (1983), and Iben (1993), together with the fact that low-mass red giants evolve in a nuclear timescale and develop the most extreme case of giantness, clearly show that thermal instabilities in the envelope are not what pushes stars into red giant dimensions. In fact, as pointed out by Faulkner (1997), even when they expand in thermal timescales envelopes lag behind, rather than lead, as can be tested by shutting off chemical changes in a stellar evolution code and letting the envelope reach its final steady-state solution consistent with the structure of the core. One of the most insightful presentations to date was given by Faulkner (2005) who describes *giantness* as a structural property of thermal equilibrium solutions consisting of a compact core, the presence of a burning shell, and a massive envelope that imposes a “mass storage problem” to the star. The fact that it is a structural property of thermal equilibrium solutions does not imply that a star out of thermal equilibrium cannot be in a giant configuration, but just that in those cases we should understand them as evolving toward the corresponding structure in thermal equilibrium in a Kelvin–Helmholtz timescale. In his article, Faulkner (2005) proceeds first by defining a set of principles of stellar structure and the meaning of a dense core. Then, assuming a simple model with a discontinuity at the burning shell, proceeds to derive an “asymptotic theory” of low-mass red giants. For this, he first motivates that the temperature at the discontinuity follows a very specific relation (his Equation (10.2)) with the help from polytropic envelope integrations (performed in his Appendix 10. A.2). From these expressions, and using some numerical results of polytropic envelope integrations, he argues that massive envelopes have forcefully a very small value of his parameter τ , which effectively means that temperature at the burning shell has a tight dependence on the mass and radius of the core. Using this result, he then derives two “theorems” for how the luminosity of the star and the density of the shell relate to the mass and radius of the core—his Equations (10.7) and (10.8); the latter is only valid for a very specific temperature dependence of the energy generation rate. Once this is done, he proceeds to extend his results to a unified treatment of main-sequence stars and red giants, horizontal branch stars, and finally to giant stars with luminous cores. However, we understand the work by Faulkner (2005) to be problematic due to a florid but mathematically obscure presentation, and the reliance on assumptions difficult to justify. Among these, his derivation of his Equations (10.5) and (10.18) stick out, as their derivation require that $P_{\text{rad}}/P_{\text{gas}}$ is constant throughout the burning shell, but nonzero, imposing a relation between T^4 and P , which disappears when radiation pressure is negligible.³ Another feature that makes his Equation (10.5) suspicious is the fact that the energy generation from the burning shell is proportional to the cube of the radius of the burning shell, while in a thin shell approximation the expected dependence would be with the square of the radius. More worrying is the fact that, within his asymptotic theory, the core mass–luminosity relation (his Equation (10.7)) is obtained without any mentioning regarding the development of convection in the envelope. This result is a consequence of the assumption, in his asymptotic theory, that $\tau = 0$, which is not rigorously demonstrated and only based on

³ Which implies that $1-\beta$ is close to zero. Oddly enough radiation pressure is negligible in the conditions relevant for red giants, and the appearance of the $1-\beta$ factor is rather disturbing.

the discussion of polytropic envelopes on the U - V plane. In fact, it has been known since the work of Sandage & Schwarzschild (1952) that, without the inclusion of an outer convective region, post main sequence post-main-sequence models expand without increasing their luminosity (see for example Figure 3 in Sandage & Schwarzschild 1952 and Figure 2 of Stancliffe et al. 2009). These issues, together with his assumption of a very specific temperature dependence for the CNO cycle ($\eta \simeq 15$; his Equations (10.8) and (10.10)), his use of the U - V plane (in his Appendix 10.A.2), and his emphasis on polytropic envelopes (particularly the $n = 3$ polytrope), makes his final conclusions difficult to accept. In spite of these mathematical shortcomings, we believe his perceptive physical description of the red giant structure is worth exploring.

The aim of this paper is to present a compelling toy model of red giants that improves our insight of how these stars work. Note in passing that the key feature of toy models is not precision but the accurate description of the main processes involved,⁴ albeit distilled to its most simple elements. This is the ideal we pursue through the paper. The paper is structured as follows: first on Section 2 we analyze the burning shell and its surroundings. This sets the key constraints imposed by the burning shell and the envelope on the thermodynamic variables. Moreover, this section offers the first proof we are aware of for the underlying hypothesis of the so-called shell homology relations; i.e., that temperature (T_s), pressure (P_s), density (ρ_s) at the location of the burning shell only depend on the radius (R_s) and mass (M_c) of the core. In addition, these sections will clarify the problems with some assumptions behind Faulkner’s asymptotic theory and highlight the role of convection in the outer layers. Then on Section 3 we check the accuracy of the derived expressions by constructing a toy model of a full low-mass red giant and compare its predictions with those of detailed stellar evolution computations. Interestingly this toy model helps us understand why all low-mass stars develop the Helium flash at nearly the same core mass, why this mass is about a half a solar mass, and why the burning shell in low-mass stars remains at an almost constant location through the evolution. After this validation, on Section 4 we make a dimensional analysis of red giant stars of all masses. Dimensional analysis of the resulting expressions shows why the presence of a burning shell makes homologous contraction of the whole star impossible and forces the formation of bright red giants. A simple description of the formation of red giants at all masses is presented on Section 5. We conclude the paper by summarizing our results and the physical insights gained from the present model. We hope that the last two sections will convince our most numerically minded readers of why simple models can improve our understanding of the inner workings of stars, even after so many decades of numerical simulations.

2. The Burning Shell and its Surroundings

One of the defining features of a red giant star is the presence of a very localized burning shell. Figure 1 shows a schematic description of the region of the star around the burning shell.⁵

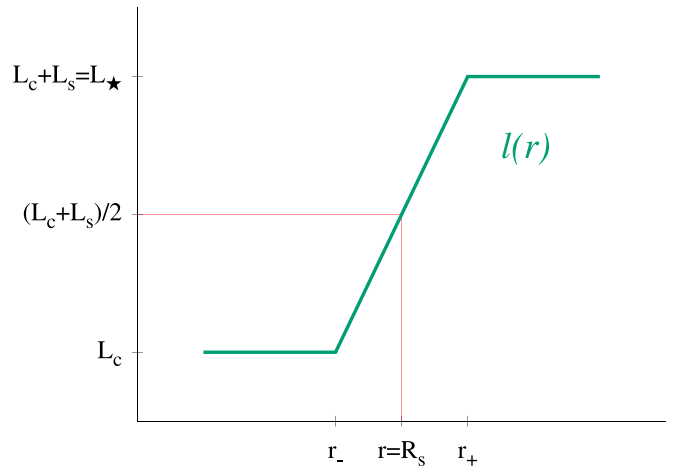


Figure 1. Schematic description of the evolution of the luminosity $l(r)$ around the burning shell for a core with generic luminosity L_c . Note that r_- and r_+ indicate the position of the inner and upper boundaries of the burning shell, and L_s indicates the total energy per unit time generated in the burning shell.

We will indicate by T_- , P_- , ρ_- , and r_- the structure variables at the bottom boundary of the burning shell, and by T_+ , P_+ , ρ_+ , and r_+ those at the upper boundary of the burning shell. Energy generation happens between r_- and r_+ , where the luminosity l increases from the luminosity of the core (L_c) to the luminosity of the envelope ($L_c + L_s$). R_s indicates the location of the middle of the burning shell, where the thermodynamic variables are T_s , P_s , ρ_s . Note that for a burning shell to have an impact on the structure of the star its luminosity must be at least similar to that of the core ($L_s \gtrsim L_c$). In the most interesting cases in fact L_s will be $L_s \gg L_c$. Due to the extreme sensitivity of nuclear reaction rates with the temperature (e.g., $\epsilon_{\text{CNO}} \simeq \epsilon_0 \rho^t T^\nu$, with $t = 1$, and $\nu \simeq 23-10$ for $T \simeq 10^7-10^8$ K), a small decrease in the temperature is enough to produce a huge drop in the energy generation rate. A small decrease of $\delta T/T \simeq 1/\nu$ leads the energy release to drop almost to zero $\delta \epsilon/\epsilon \simeq \nu \delta T/T \simeq 1$. As a consequence the energy released by the burning shell is concentrated in a thin region of $\sim 2\delta T$ around the characteristic temperature of the shell T_s . This will allow us to work with first-order approximations around the shell temperature $f(T_s + dT) \simeq f(T_s) + \frac{df}{dT}(T_s)dT$ and consider the burning shell to be thin for most computations (i.e., $r_- \simeq R_s \simeq r_+$).

Due to the presence of the H-burning shell, the stellar plasma at the shell cannot be degenerate.⁶ Then, as the material on the burning shell is not degenerate, and T , ρ , and P are continuous, there *must* exist regions, immediately below and above the burning shell, where the material behaves as a classical ideal gas ($P = \mathfrak{R}\rho T/\mu$).⁷

2.1. Above the Burning Shell

As a first step on our way to understanding the physics of red giants, we will look at how the outer boundary conditions establish some constraints on the thermodynamical quantities immediately above the burning shell. In particular, we will see

⁴ “All models are wrong but some are useful” Box (1979).

⁵ Note that our treatment of the burning shell is rather different from that of Faulkner (2005). In that work the burning shell was adopted as a discontinuous transition making no distinction between the values of the variable below, at and above the burning shell. In view that some of these variables can have significant changes (e.g., $L_c \ll L_s$), we think that approximation is not justified.

⁶ Otherwise a flash would develop, injecting huge amounts of energy in that layer and lifting degeneracy.

⁷ Strictly speaking as a classical ideal gas plus radiation, but radiation pressure always plays a minor role at the burning shell. In fact, we know from observations that most giant stars are far from the Eddington luminosities of their cores.

that the outer boundary conditions strongly restrict the possible values of the temperature gradient $\nabla = d \ln T / d \ln P$.

Under the assumption that the envelope is in a steady state (thermal equilibrium, $dS/dt \simeq 0$, $\int_0^{M_*} |\epsilon_g| dm \ll L_*$), the thermodynamic variables in the envelope above the burning shell must fulfill the hydrostatic equilibrium equation,

$$\frac{dP}{dm} = -\frac{Gm}{4\pi r^4}, \quad (1)$$

the connection between the local radius and the Lagrangian mass coordinate,

$$\frac{dr}{dm} = -\frac{1}{4\pi r^2 \rho}, \quad (2)$$

and the heat transport equation,

$$\frac{dT}{dm} = -\frac{GmT}{4\pi r^4 P} \nabla. \quad (3)$$

In the last equation ∇ is given by

$$\nabla = \nabla_{\text{rad}} = \frac{3}{16\pi acG} \frac{\kappa L_* P}{mT^4}, \quad (4)$$

when $\nabla_{\text{rad}} < \nabla_{\text{ad}}$ and energy is transported by radiation, or $\nabla = \nabla_{\text{ad}}$ when convection develops (Schwarzschild 1906). All quantities in Equations (2), (3), and (4) have been defined as in the classic textbook by Kippenhahn et al. (2012), and $L_* = L_s + L_c$ is the luminosity of the star.

Given that we want to understand the general properties imposed by the envelope on the burning shell for a core of arbitrary mass (M_c) and radius (R_s) it is convenient to use adimensional variables. Using the mean pressure of the core \bar{P}_c , the mean density of the core $\bar{\rho}_c$, and a characteristic temperature T_c ⁸,

$$\bar{P}_c = \frac{GM_c^2}{8\pi R_s^4}, \quad \bar{\rho}_c = \frac{3}{4\pi} \frac{M_c}{R_s^3}, \quad T_c = \frac{\mu GM_c}{6\mathfrak{R}R_s}, \quad (5)$$

we define $q = m/M_c$, $x = r/R_s$, $y = P/\bar{P}_c$, $z = \rho/\bar{\rho}_c$, and $t = T/T_c$. Assuming that the gas is a classical ideal gas and that the opacity can be approximated by a power law $\kappa = \kappa_0 P^a T^b$ ($a \geq 0$, $b \leq 0$ under normal conditions), Equations (1), (2), (3), (4) can be written as

$$\frac{dy}{dq} = \frac{-2q}{x^4}, \quad \frac{dx}{dq} = \frac{t}{3x^2y}, \quad \frac{dt}{dq} = \mathbb{C} \frac{y^a t^{b-3}}{x^4}, \quad (6)$$

and

$$\nabla = \min \left(\mathbb{C} \frac{y^{a+1} t^{b-4}}{-2q}, 0.4 \right). \quad (7)$$

The meaning of the constant \mathbb{C} ($\mathbb{C} < 0$) can be made clear by defining a characteristic luminosity⁹ L_0 for a core of mass M_c and radius R_s as

$$L_0 = \frac{64\pi^2 ac}{3} \frac{T_c^4 R_s^4}{M_c \kappa_c}, \quad (8)$$

⁸ Defined as the temperature of a classical ideal gas with the mean hydrostatic pressure \bar{P}_c and mean density $\bar{\rho}_c$ of the core.

⁹ The reader is warned not to confuse L_0 , which is a reference luminosity for a core of given mass and radius, with the luminosity of the core L_c to be defined in the next sections.

where $\kappa_c = \kappa(\bar{P}_c, T_c)$. With this definition it becomes clear that \mathbb{C} is an adimensional version of the luminosity of the star and $\mathbb{C} = -L_*/L_0$.

Due to hydrostatic equilibrium pressure at the burning shell is necessarily lower than the mean pressure at the core, and even more so at the top boundary of the burning shell ($y_+ < 1$, and much lower than unity for dense cores). On the other hand, as temperature does not change significantly across the burning shell it is usually $t_+ \lesssim 1$. Note that as T_c corresponds to the temperature required by a classical ideal gas at the mean density of the core to match the hydrostatic pressure, for degenerate cores T_c is actually larger than the real temperature of the core and thus of the shell, and then $t_+ < 1$. We can get a clear idea of the relevant values of \mathbb{C} by replacing the quantities in Equation (8) with those of a typical envelope ($\mu \simeq 1.176$, $\kappa \sim 0.34 \text{ cm}^2 \text{ g}^{-1}$) and obtain,

$$L_0 = 6.77 \times 10^{35} \left(\frac{M_c}{M_\odot} \right)^3 \text{ erg/s} = 177 \left(\frac{M_c}{M_\odot} \right)^3 L_\odot. \quad (9)$$

We see from Equation (9) that for typical values of core masses in red giants, L_0 is lower than the typical luminosities of the same stars on the main sequence. Physically interesting values of \mathbb{C} correspond to $\mathbb{C} \gtrsim 1$ and even $\mathbb{C} \gg 1$ in the case of low-mass stars.

Using Equation (6) we can integrate the envelopes from the upper boundary of the burning shell (y_+, t_+) outward. Note that one of the key assumptions here is that the envelope is massive enough so that we can integrate outward in q without reaching the photosphere (up to 30% of the core mass in Figure 2). Figure 2 shows the result of these envelope integrations for $y_+ \in (10^{-4}, 0.5)$, $\log|\mathbb{C}| \in (-1, 5)$ and for a Kramers' opacity law ($a = 1$ and $b = -4.5$). Similar results are obtained for a classical Thomson electron scattering opacity ($a = 0$ and $b = 0$) and other values of $t_+ \sim 1$ (see Appendix D).

As it is clear from Figure 2, two main families of solutions are possible. Solutions in black correspond to solutions in which the radiative gradient increases as we move outward from the burning shell. In most cases these envelopes become convective ($\nabla = 0.4$). Conversely, solutions in orange correspond to those cases in which the radiative gradient drops extremely fast as we move outward (in fact more than exponentially as can be seen in Figure 2). As shown in Figure 2, these solutions quickly become isothermal at a temperature close to that of the shell. This second family of solutions does not correspond to physical stellar envelopes as they cannot satisfy photospheric boundary conditions. Using Eddington's approximation we know that $d \log T / d\tau|_{\text{ph}} \simeq 3/16$ and from a zero-order integration for the pressure $d \log P / d\tau|_{\text{ph}} \simeq 3/2$, and consequently the temperature gradient near a stellar photosphere must be $\nabla_{\text{ph}} \sim 1/8$. Such a condition cannot be satisfied by the orange solutions that stay radiative throughout the whole integration as ∇_{rad} decreases monotonically, and for which $\nabla_{\text{rad}} \ll 1$ very close to the core. Interestingly, the watershed between both families of solutions corresponds to those envelopes that start at the burning shell with a temperature gradient of $\nabla_+ = (a+1)/(4-b)$ (shown as a blue horizontal line in Figure 2).

To better understand this behavior it is instructive to look at the derivative of the temperature gradient. Using Equations (6) and (7), it is easy to show that

$$\frac{d\nabla_{\text{rad}}}{d \log q} = \nabla_{\text{rad}} \left[((a+1) + (b-4)\nabla_{\text{rad}}) \frac{d \log y}{d \log q} - 1 \right], \quad (10)$$

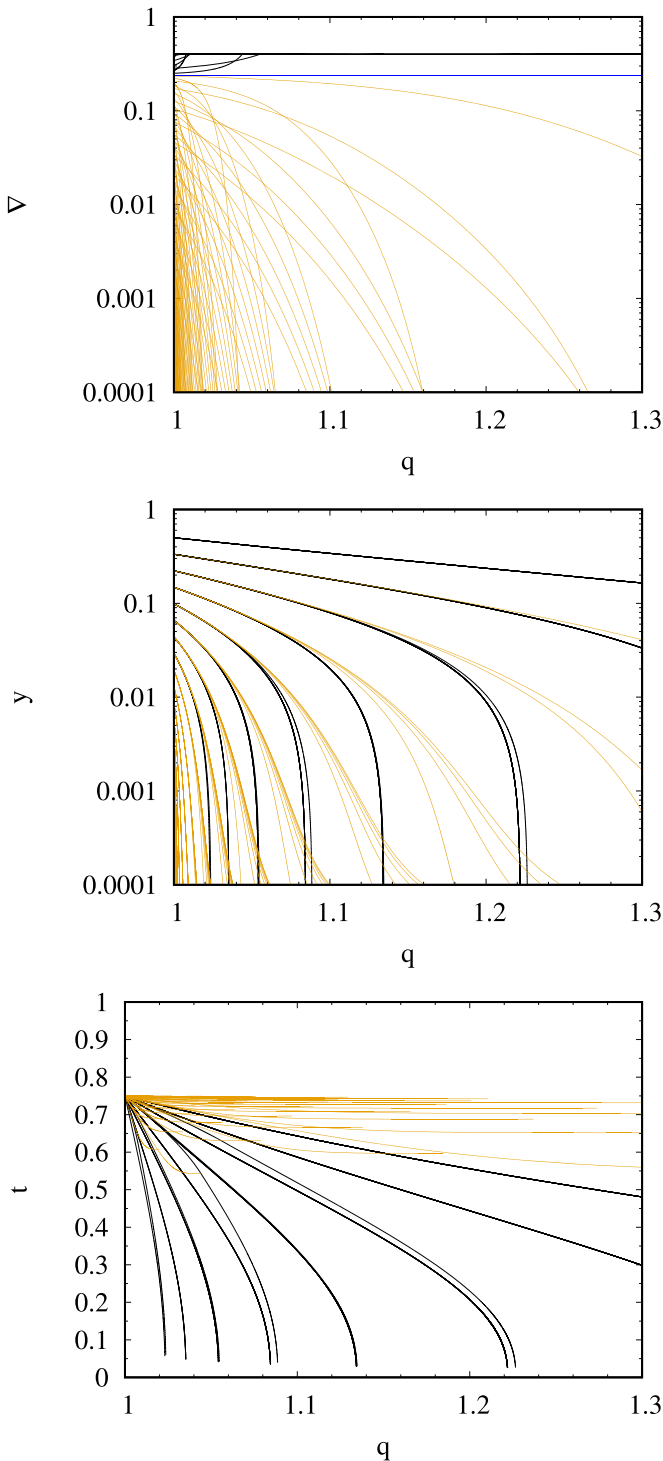


Figure 2. Envelope integration for different values of \mathbb{C} and y_+ , for $t_+ = 0.75$ and for a Kramers' opacity.

where due to hydrostatic equilibrium $d \log y / d \log q < 0$. It is now clear that if $\nabla_{\text{rad}} \leq (a+1)/(4-b)$ at some point, then Equation (10) behaves locally as $\frac{d\nabla_{\text{rad}}}{d \log q} = \mathbb{A} \times \nabla_{\text{rad}}$ with $\mathbb{A} < 0$ and ∇_{rad} drops exponentially. Then solutions with $\nabla_{\text{rad}} \leq (a+1)/(4-b)$ already at the burning shell are not physical. Physically meaningful solutions are then confined to values of $\nabla > (a+1)/(4-b)$. On the other hand, due to convection we know that the temperature gradient cannot exceed the adiabatic value. Then, we have shown that the outer

envelope imposes a very strict constraint on the value of the temperature gradient in the envelope, and immediately above the burning shell $-(a+1)/(4-b) < \nabla < 0.4$.

Interestingly, as it can be guessed from Figure 2, physical solutions with ∇_+ near the adiabatic value will correspond to envelopes that turn convective very quickly (deep convection). We see that, unless we are in the case of deep convection, with the bottom of the convective envelope closer than $q \sim 1.1$, the temperature gradient stays close to the critical limit $\nabla^{\text{lim}} = (a+1)/(4-b)$. Those solutions with values of ∇_+ near $(a+1)/(4-b)$ will show relatively massive radiative regions on top of the burning shell and can even stay radiative until they reach the photosphere.¹⁰ In addition, one shared property of all physical solutions is that they show a significant decrease in temperature outside the burning shell and a very strong decrease in pressure, in particular for those solutions that start with $y_+ \ll 1$. In Appendix C we show that if the convective zone reaches all the way to the burning shell, then detailed models predict a completely different behavior and a much smaller radius.

Most importantly, for typical opacity laws we have $\nabla^{\text{lim}} = 0.25$ (Thomson electron scattering, $a=b=0$) and $\nabla^{\text{lim}} = 0.2353$ (Kramers' opacity, $a=1, b=-4.5$). This means that the value of ∇ above the burning shell varies less than a factor of 2 throughout the envelope. This result will be very useful to make simple estimations in the next sections.

We end this section noting that, although these conclusions are strictly valid for an opacity that follows a power law, the conclusions are quite general. In fact, for any opacity law we can locally approximate it by a power law ($\kappa \simeq \kappa_0 P^{a'+1} T^{b'-4}$). Due to the faster-than-exponential nature of Equation (10) if ∇ drops, in some region, below the local critical value then the envelope solutions will quickly become unphysical. As a consequence, in envelopes with real opacity laws ∇ needs to stay between the local critical value $\nabla^{\text{lim}} = (a'+1)/(4-b')$ and the adiabatic value ∇_{ad} . In particular, for real envelopes near the burning shell we will have in most cases $\nabla_+ \simeq (a+1)/(4-b)$ and only for deep convection $\nabla_+ \simeq \nabla_{\text{ad}}$.

2.2. Temperature Gradient Inside the Burning Shell

Having shown in Section 2.1 that $(a+1)/(4-b) \lesssim \nabla_+ \lesssim 0.4$ we now turn to analyze how ∇ changes inside the burning shell where $l(r)$ is not constant anymore (see Figure 1).

From Equations (1) and (3) we see that inside the burning shell we have

$$\frac{dT}{dP} = \frac{3}{16\pi a c G m T^3} \frac{\kappa l}{T}. \quad (11)$$

Using again that the opacity inside the shell follows $\kappa = \kappa_0 P^{a'} T^{b'}$ we can write

$$\frac{T^{4-b'}}{P^{a'+1}} \nabla \frac{1}{l} = \mathbb{K}, \quad (12)$$

where $\mathbb{K} > 0$ is a constant.

¹⁰ It is worth noting that solutions with $\nabla_+ > (a+1)/(4-b)$ are not forced to increase monotonically and can start to decrease depending on the local value of $\frac{d \log y}{d \log q}$. In fact, we know from integrations of photospheric conditions immediately below the photosphere that $\nabla_{\text{rad}} \simeq \tau/(\tau+2/3)$, where τ is Rosseland optical depth.

Evaluating the left-hand side of Equation (12) both at the upper boundary and the center of the shell, we obtain

$$\nabla_+ = \left(\frac{T_s}{T_+} \right)^{4-b} \left(\frac{P_+}{P_s} \right)^{a+1} \nabla_s \frac{L_c + L_s}{L_c + L_s/2}. \quad (13)$$

We know from the high sensitivity of the energy generation to temperature that temperature changes only slightly inside the burning shell $T_s - T_+ = \Delta T = T_s/\nu$. Let us call $x = \Delta P/P_s$ ($P_+ = P_s(1-x)$), then $dP/P = (\nabla_s)^{-1} dT/T$, and we see that $x = (\nabla_s \nu)^{-1}$. Note that, as $\Delta T/T_s \ll 1$ and $(a+1)/(4-b) \lesssim \nabla_+ \lesssim 0.4$ then also $x \ll 1$ for typical values of the opacity. Then Equation (13) can be written as

$$\nabla_+ = \left(1 + \frac{1}{\nu} \right)^{4-b} (1-x)^{a+1} \frac{1}{x\nu} \frac{L_c + L_s}{L_c + L_s/2}. \quad (14)$$

Defining F as the factor due to the luminosity of the core, $F = (L_c + L_s)/(L_c + L_s/2)$ ($F = 2$ for inert cores), we can write at first order in $1/\nu$

$$\nabla_+ = \left\{ 1 + \left(\frac{4-b}{\nu} \right) \times \left[1 - \left(\frac{a+1}{4-b} \right) \frac{1}{\nabla_s} \right] + \mathcal{O}(1/\nu^2) \right\} F \nabla_s. \quad (15)$$

We see here that the dominant factor for $\nu \gg 1$ is due to the change in the luminosity throughout the shell (F) and that at the dominant order the value of ∇_s is

$$\nabla_s \simeq \frac{\nabla_+}{F} = \left[\frac{1/2 + L_c/L_s}{1 + L_c/L_s} \right] \nabla_+. \quad (16)$$

We see that the temperature gradient is changed by a relative large factor F^{-1} in the small region of the burning shell. In particular, for an inert core ($F = 2$, $L_c \ll L_s$) and the value of ∇_s becomes half its value at the upper boundary. Like ∇_+ , ∇_s is also tightly constrained by the outer envelope.

If we now estimate ∇_- , we see that the temperature gradient at the bottom of the burning shell is

$$\nabla_- \simeq \left[\frac{L_c}{L_s + L_c} \right] \nabla_+, \quad (17)$$

where it becomes clear that in the case of the inert core $L_c \ll L_s$ the material becomes isothermal at the lower boundary of the burning shell, as we know from numerical models of low-mass stars (see Appendix A).

Knowing the value of ∇_s we can make some useful estimations of how pressure and density change across the burning shell. Using that at the burning shell $dP/P \simeq (\nabla_s)^{-1} dT/T$ and using the equation of state of an ideal gas we get

$$P_+ \simeq P_- \exp \left[\frac{-2F}{\nu \nabla_+} \right], \quad (18)$$

$$\rho_+ \simeq \rho_- \frac{\mu_{\text{env}}}{\mu_{\text{core}}} \exp \left[\frac{-2}{\nu} \left(\frac{F}{\nabla_+} - 1 \right) \right],$$

where μ_{env} and μ_{core} are the mean molecular weights of the envelope and core, respectively.

2.3. The Upper Mantle and the Drop in P , ρ , and T Above the Burning Shell

We now turn to analyze how the radiative region above the burning shell (from now on, the upper mantle) imposes some tight constraints on the thermodynamical quantities at the upper boundary of the burning shell, and consequently on the burning shell itself.

Let us first note that due to hydrostatic equilibrium the drop in pressure and temperature immediately above the burning shell is

$$\frac{dP}{P} \Big|_+ = \frac{\bar{P}_c}{P_+} \frac{dm}{M_c}, \quad \frac{dT}{T} \Big|_+ = \frac{\bar{P}_c}{P_+} \nabla_+ \frac{dm}{M_c}. \quad (19)$$

This implies that, as the core becomes more compact and the pressure contrast between the upper boundary of the shell and the core increases by orders of magnitude ($\bar{P}_c \gg P_+$), the drop in pressure and temperature above the shell will become large even in a region of almost negligible mass ($\Delta m/M_c = (m - M_c)/M_c \ll 1$). In the following we will show that, when this happens, very tight constraints on the burning shell can be derived. Then we will show that these constraints are approximately valid even at the very early stages of shell burning (i.e., immediately after the end of the main sequence).

One of the key results from Section 2.1 is the fact that ∇ is strictly constrained above the burning shell to values $(a+1)/(4-b) < \nabla < 0.4$, which in practice prevents ∇_+ from varying more than a factor 2 in that region. If we now restrict ourselves to a region of negligible mass above the burning shell ($\Delta m/M_c \ll 1$) we can approximate

$$\frac{dT}{dr} \simeq - \frac{-\mu_{\text{env}} G M_c \bar{\nabla}}{\mathfrak{R} r^2} \frac{1}{r^2}, \quad (20)$$

where $\bar{\nabla}$ is typical mean value of ∇ that fulfills $(a+1)/(4-b) < \bar{\nabla} \leq 0.4$. Integrating this expression downward from a point ($r = R_0$) where our approximations are still valid we can obtain

$$T \simeq \frac{G M_c \mu_{\text{env}} \bar{\nabla} (1 - r/R_0)}{r \mathfrak{R} (1 - T_0/T)}. \quad (21)$$

We see that in those cases where T , ρ , and P drop significantly in a massless region above the burning shell, this is when the core becomes compact in the sense that $\bar{P}_c \gg P_+$; then we can move outwards to a point $R_0 \gg r$ and $T_0 \ll T$, and the factors on the right-hand side of Equation (21) become close to unity. We will see below, however, that even under not very extreme conditions, the factors on the right are of order 1.

In particular, Equation (21) sets a tight relation for the temperature immediately above the burning shell,

$$T_+ \simeq \frac{G M_c \mu_{\text{env}} \bar{\nabla} (1 - R_s/R_0)}{R_s \mathfrak{R} (1 - T_0/T_+)}. \quad (22)$$

Again, here the adimensional factor $(1 - R_s/R_0)$ will approach unity fast, as the density contrast between the shell and the core increases, as when $\rho_+ \ll \rho_c$ it is possible to integrate outward to large values of R_0 keeping the approximation $m \simeq M_c$. It will be shown later that even in the early stages of shell burning these adimensional factors are all close to unity. It is then useful to

write all the factors close to one as¹¹

$$T_+ \simeq \frac{G M_c \mu_{\text{env}} \bar{\nabla} \zeta}{R_s \mathfrak{K}}, \quad (23)$$

where ζ will be very close to one¹² and $(a+1)/(4-b) < \bar{\nabla} \leq 0.4$. We will see below that when the density and pressure drop by orders of magnitude in a massless region above the burning shell, then $\bar{\nabla} \simeq (a+1)/(4-b)$.

It is useful to note that, when the factors on the right in Equation (21) can be neglected we also have that

$$\frac{d\rho}{dr} \simeq -\frac{\rho}{r}(1-\bar{\nabla})\frac{(1-T_0/T)}{(1-r/R_0)}. \quad (24)$$

To have a more quantitative idea of the implications in Equations (21), (23), and (24) we can assume that energy is transported by radiation in the region immediately above the burning shell. Note that if energy is transported by convection the situation is straightforward as then ∇ is completely constant and $\nabla=0.4$. Again, if we restrict to a region where $\Delta m/M_c \ll 1$, we can replace Equation (1) into Equation (3) and obtain

$$dT = \frac{3L_*}{16\pi a c G M_c T^3} dP. \quad (25)$$

Writing the opacity dependence close to the burning shell as $\kappa = \kappa_0 P^a T^b$ ($a \geq 0$, $b \leq 0$ under normal conditions), Equation (25) can be integrated in the standard way (Kippenhahn et al. 2012) from a point ($r=R_0$) where our approximation is still valid down to the burning shell

$$(T_0^{4-b} - T^{4-b}) = \frac{4-b}{a+1} \frac{3\kappa_0 L_*}{16\pi a c G M_c} (P_0^{a+1} - P^{a+1}). \quad (26)$$

We can see now that the value of ∇ inside the upper mantle is

$$\nabla = \frac{(4-b)[1-(T_0/T)^{4-b}]}{(a+1)[1-(P_0/P)^{a+1}]} \quad (27)$$

Under these conditions, the temperature and density at the upper boundary of the burning shell must fulfill

$$T_+^{4-b} = \frac{\Pi}{\Theta} \frac{4-b}{a+1} \frac{3\kappa_0 L_*}{16\pi a c G M_c} P_+^{a+1}, \quad (28)$$

with $\Theta = (1 - (T_0/T_+)^{4-b})$ and $\Pi = (1 - (P_0/P_+)^{a+1})$. As before, as soon as $P_c \gg P_s$, pressure and temperature drop quickly above the burning shell and $\Theta/\Pi \simeq 1$. The value of ∇

¹¹ It is worth noting that, while Equation (23) has similarities with Equation (10.2) in Faulkner (2005; when $\tau=0$), they rely on very different justifications. While the assumption of $\tau \simeq 0$ in Faulkner (2005) is based on the analysis of polytropic envelope integrations in the U-V plane with no discussion about the role of convection, Equation (23) is based on the analysis done in Section 2.1. One of the key ingredients in the derivation of Equation (23) is the fact that the development of convection together with outer boundary conditions strongly constrain the value of ∇ . This highlights the role of convection in the formation of bright red giants and explains why the early models that neglected the existence of convection (Sandage & Schwarzschild 1952) did not form luminous red giants.

¹² It must be emphasized that the argument presented in the next sections does not require $\zeta=1$ but only that ζ is of order 1, even if within a factor of a few. The important feature is that $\bar{\nabla}\zeta$ is tightly constrained, and Equation (23) sets an effective constraint between T_+ , M_c , and R_s . In fact the case of $\zeta=1$ corresponds to the case when boundary terms can be neglected and ρ , T , and P can be assumed to have a simple power-law dependence on r , leading to a polytropic relation among them (see Chapter Section 19.2 in MacDonald 2015).

at the upper boundary of the burning shell is then

$$\nabla_+ = \left. \frac{d \ln T}{d \ln P} \right|_+ = \frac{a+1}{4-b} \frac{\Theta}{\Pi}. \quad (29)$$

Then, once $\Theta \simeq 1$ and $\Pi \simeq 1$ we see that typical values of $\bar{\nabla} \simeq \nabla_+ \simeq (a+1)/(4-b)$ are 4/17 for a Kramers' opacity and 1/4 for Compton scattering.

Interestingly, the envelope integrations discussed in Section 2.1 show that this also applies to massive radiative envelopes for which we cannot approximate $m \simeq M_c$ through all the integration. This is because ∇ , due to Equation (10), needs to stay close to $\nabla^{\text{lim}} = (a+1)/(4-b)$ to avoid a runaway increase in ∇ , which would turn the envelope convective, but also larger than this critical value to avoid a runaway drop in ∇ , which would make it impossible to satisfy photospheric boundary conditions.

As discussed above, when $\rho_+ \ll \rho_c$ and $P_+ \ll P_c$ we can strictly demonstrate that $\Theta \simeq 1$, $\Pi \simeq 1$, $\zeta \simeq 1$, $T_0 \ll T_+$ and $R_s \ll R_0$, and all previous expressions are very simple. In Appendix E, we show that these approximations are still acceptable in the early stages of the burning shell, when the pressure and density contrast are not that large. Readers not inclined to these rough estimations can skip this appendix and wait for Section 3.2, where the predictions of these approximation will be compared, and validated, against full stellar evolution models.

2.4. Energy Release at the Burning Shell

A second relation between the temperature gradient, temperature, density, and shell luminosity can be derived from the fact that L_s is the consequence of the energy generated in the shell itself. From the energy conservation equation

$$\frac{dl}{dm} = \epsilon, \quad (30)$$

we can estimate that $L_s \simeq \langle \epsilon \rangle \Delta m = \langle \epsilon \rangle \rho_s 4\pi R_c^2 \Delta r$. Noting that almost all energy is released in a region where $\delta T/T \simeq 2/\nu$ (T_s/ν corresponds to half a burning shell), we can use that $\Delta r \simeq -(dT/dr)^{-1} 2 T_s/\nu$

$$L_s = \langle \epsilon \rangle 4\pi R_c^2 \rho_s \frac{-T_s 2}{\nu} \left(\frac{dT}{dr} \right)^{-1}. \quad (31)$$

Given that energy transport at the burning shell happens through radiation, we can estimate that the temperature gradient at the peak of the H-burning shell, i.e., in the middle of the burning shell where $l_{\text{mid-shell}} = L_c + L_s/2 = (L_s/2)(1 + 2L_c/L_s)$, also fulfills

$$\left. \frac{dT}{dr} \right|_{\text{shell}} \simeq \frac{-3}{16\pi a c} \frac{\kappa_s \rho_s}{R_c^2 T_s^3} (L_s/2 + L_c). \quad (32)$$

Replacing L_s from Equation (32) into Equation (31), and noting that the mean energy release is about half its value at the peak¹³, $\langle \epsilon \rangle \simeq \epsilon(\rho_s, T_s)/2 \simeq \epsilon_0/2 \rho_s^i T_s^{\nu}$, and replacing that in

¹³ This is exact for a linear luminosity increase in the shell.

Equation (3) we have

$$\left(\frac{dT}{dr}\Big|_{\text{mid-shell}}\right)^2 \simeq \frac{3}{8ac\nu} \left(\frac{\rho_s}{T_s}\right)^2 \times \kappa(\rho_s, T_s) \epsilon(\rho_s, T_s) \left(1 + \frac{2L_c}{L_s}\right) \quad (33)$$

or

$$\left(\frac{dT}{dr}\Big|_{\text{mid-shell}}\right)^2 \simeq \frac{3}{8ac} \frac{\kappa_0 \epsilon_0 \mathfrak{R}^a}{\mu^a} \times \frac{\rho_s^{2+s+t} T_s^{a+b+\nu-2}}{\nu} \left(1 + \frac{2L_c}{L_s}\right). \quad (34)$$

2.5. Constraints Set by the Burning Shell on the Thermodynamic Variables

Equations (33) and (34) tell us how the temperature gradient has to be, for the total energy of the shell to be released in a region where temperature drops by $\sim 2T_s/\nu$. In addition to Equations (33) and (34), due to the radiative transport and hydrostatic equilibrium equations we know that at location $r = R_s$, the temperature gradient must be such that it transports the local luminosity of the star at that point. This is

$$\begin{aligned} \frac{dT}{dr}\Big|_{\text{mid-shell}} &= \nabla_s \frac{T_s}{P_s} \left(\frac{dP}{dT}\Big|_{\text{mid-shell}}\right) \\ &= \frac{\nabla_+}{F} \times \left(\frac{-GM_c \mu_s}{R_s^2 \mathfrak{R}}\right). \end{aligned} \quad (35)$$

Equating the gradients $dT/dt(\text{mid} - \text{shell})$ in Equations (33) and (35) we find that the existence of the burning shell forces

$$\begin{aligned} &\left(\frac{-GM_c \mu_s}{R_s^2 \mathfrak{R}}\right)^2 \left(\frac{1 + \frac{2L_c}{L_s}}{1 + \frac{L_c}{L_s}}\right)^2 \times (\nabla_+)^2 \\ &= \frac{3}{2ac\nu} \left(\frac{\rho_s}{T_s}\right)^2 \kappa(\rho_s, T_s) \epsilon(\rho_s, T_s), \end{aligned} \quad (36)$$

where we have replaced the factor $1/F$ by its dependence on the luminosity to emphasize the behavior of the equation in the case of luminous shells $L_c/L_s \ll 1$. Equation (36) is the key equation to understand the behavior of the stellar structure in the presence of a burning shell.¹⁴ We have seen that $(a+1)/(4-b) < \nabla_+ < \nabla_{\text{ad}}$ and, as soon as their core becomes dense $\nabla_+ \simeq (a+1)/(4-b)$ (Equation (29)). The first thing to note is that in the case of a dim shell ($L_s \ll L_c$), this equation becomes meaningless (in fact) as it only implies that $\epsilon_s \simeq 0$, which is a trivial result as nothing should happen in that situation. As soon as the energy generated in the burning shell becomes relevant ($L_s \sim L_c$), Equation (36) starts to put constraints on the values of T_s and ρ_s as a function of the mass and radius of the core (M_c, R_s). We see that the key

¹⁴ Equation (36) is closely related to Equation (10.5) in Faulkner (2005). However, here the weird dependence on the cube of the radius of the burning shell has been replaced by the more reasonable R_s^2 , and the weird appearance of the radiation density constant has been removed. In addition, the explicit appearance of ∇_+ highlights the role of the constraints imposed by the envelope.

consequence of the development of a burning shell is the emergence of an additional constraint (Equation (36)), between ρ_s, T_s , and R_s and M_c .

To fully appreciate the power of Equation (36) we need to complement it with Equation (23), a constraint that is always present in stellar envelopes. Noting that $T_s = T_+(1 + 1/\nu)$ we have

$$T_s \simeq \frac{G M_c \mu_{\text{env}}}{R_s \mathfrak{R}} (1 + 1/\nu) \nabla_+, \quad (37)$$

where we have approximated $T_0 \ll T_s$ and $R_s \ll R_0$, which according to our previous discussion are good approximations under rather general situations. This equation implies an additional constraint on T_s , and together with Equation (36) it implies that the values of T_s, ρ_s , and P_s are completely defined by the values of M_c and R_s . In fact Equations (36), and (23) demonstrate the key hypothesis in the derivations of ‘‘shell homology relations’’ (see Chapter 33.2 in Kippenhahn et al. 2012), i.e., $T_s(M_c, R_s)$, $\rho_s(M_c, R_s)$, and $P_s(M_c, R_s)$.

An alternative version of Equation (36) can be obtained by using Equation (23) on the left-hand side of Equation (36) to obtain

$$\begin{aligned} &\left(\frac{\mu_s}{\mu_e}\right)^2 \frac{\left(1 + \frac{2L_c}{L_s}\right)}{\left(1 + \frac{L_c}{L_s}\right)^2} (1 + 1/\nu)^2 \\ &= \frac{3}{2ac\nu} \left(\frac{\rho_s^2 R_s^2}{T_s^4}\right) \kappa(\rho_s, T_s) \epsilon(\rho_s, T_s). \end{aligned} \quad (38)$$

To good approximation we have

$$\left(\frac{\mu_s}{\mu_e}\right)^2 \simeq \frac{3}{2ac\nu} \left(\frac{\rho_s^2 R_s^2}{T_s^4}\right) \kappa(\rho_s, T_s) \epsilon(\rho_s, T_s). \quad (39)$$

In the next section we will test and validate all the expressions derived here by building a toy model of a low-mass red giant and comparing it to the predictions of detailed full stellar models. Before this, let us summarize what we have found so far. In Section 2.1 we have shown that the existence of an envelope of nonnegligible mass, together with the photospheric boundary conditions, imply that the temperature above the burning shell must follow $(a+1)/(4-b) \lesssim \nabla_+ \lesssim 0.4$, where $(a+1)/(4-b) \simeq 0.23-0.25$. Then, on Section 2.2 we have seen that the high temperature sensitivity of nuclear reactions and hydrostatic equilibrium can be used to show that the temperature gradient inside the burning shell is $\nabla_s \simeq \nabla_+/F$, where $F \simeq 2$ when the shell is much more luminous than the core ($L_s \gg L_c$). As shown in Section 2.3 this implies, among other things, that the temperature at the shell follows $T_s \propto M_c/R_s$. Finally, the fact that the luminosity generated at the burning shell must also be transported through the burning shell leads to a tight constraint of ρ_s and T_s as a function of M_c and R_s . Together these last two results demonstrate the validity of the key hypothesis of the so-called shell homology relations (see Chapter 33.2 in Kippenhahn et al. 2012), i.e., that we can write $T_s(M_c, R_s)$, $\rho_s(M_c, R_s)$, and $P_s(M_c, R_s)$.

3. The Validation: A Toy Model for a Low-mass Star

To better understand the equations derived in Section 2 and to check their accuracy, we will construct here a toy model of a

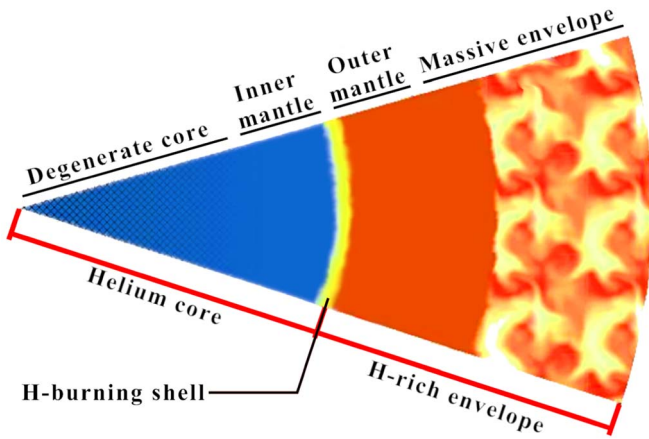


Figure 3. Main structural parts of a low-mass red giant.

low-mass red giant (Figure 3). Fortunately, the degenerate core of low-mass red giants can be approximated by a self-gravitating sphere sustained by the pressure of cold non-relativistic electrons.

A cold core supported by fully degenerate nonrelativistic electrons has a very tight mass–radius relationship that corresponds to an $n = 3/2$ polytrope. In cgs units, this relationship is

$$R_{dc} = 1.12 \times 10^{20} M_{dc}^{-1/3}. \quad (40)$$

This tight constraint indicates that the geometrical size of the core of low-mass stars only evolves due to the increase in their mass. This increase in M_c is provided by the steady burning of H at the burning shell. Consequently the radius of the degenerate core will evolve on a nuclear timescale. Then, due to the degeneracy of the He core, gravothermal energy release is to a first approximation negligible in comparison with the intensity of the H-burning shell; i.e., mathematically we can say that $L_s \gg L_c$. This fact, together with the high thermal conductivity provided by degenerate electrons will allow us to approximate the degenerate core as an isothermal, thermally relaxed ($\int_0^{M_c} \epsilon_g dm = 0$) structure with $L_c \ll L_s$.

One feature, usually neglected when discussing low-mass giants, and which is key to understand the $M_c(R_s)$ relation of low-mass red giants, is the existence of a very light mantle of nondegenerate ideal gas between the burning shell and the degenerate core. The existence of such an inner mantle can be easily motivated as follows. Due to the presence of the H-burning shell the stellar plasma at the shell cannot be degenerate.¹⁵ Then, as the material on the burning shell is not degenerate, and T , ρ , and P are continuous, there *must* exist regions immediately below the burning shell where the material behaves as a classical ideal gas ($P = \mathfrak{R} \rho T / \mu$). We will show that it plays a key role in the $M_c(R_s)$ relation of low-mass red giants even when its mass (Δm) is negligible (in the sense that $\Delta m \ll M_c$).

In low-mass stars after the end of core H burning the contraction of the tiny He core left is stopped by degeneracy, and the temperatures around the H-exhausted core reach $T_s \sim 10^7$ K. Note that this happens before the development of a

giant structure. From this point onward, the star can be described as composed of an almost pure inert He core, initially of less than a tenth of a solar mass and increasing with time, and a H-rich envelope that harbors the rest of the mass of the star, both separated by the presence of a H-burning shell. In addition the He core harbors a He mantle where the material behaves as a classical ideal gas. Such a configuration is depicted in Figure 3.

3.1. The Inner Mantle

As evolution proceeds in a nuclear timescale we can assume at first order that $L_c = 0$. The temperature profile of the inner mantle is then given by Equation (17), which for $L_c = 0$ corresponds to $\nabla_- = 0$. We see that the presence of the H-burning shell forces the existence of an isothermal mantle with $T \simeq T_- = T_s(1 + 1/\nu)$ in between the H-burning shell and the degenerate core.¹⁶ This mantle is in hydrostatic equilibrium and has to fulfill Equation (1). As long as the density does not increase significantly the isothermal mantle can be considered as an ideal classical gas. The mean molecular weight of the inner mantle corresponds to that of pure and fully ionized He ($\mu_c \simeq 4/3$). In this region the density must follow

$$\frac{d\rho}{dr} = -\frac{Gm\mu_c}{\mathfrak{R}r^2T}\rho, \quad (41)$$

and if we restrict ourselves to the outermost regions of the core, where $\Delta m(r) \ll M_c$, the equation becomes

$$\frac{d\rho}{\rho} = -\frac{GM_c\mu_c}{\mathfrak{R}T_-} \frac{dr}{r^2}. \quad (42)$$

This equation can be integrated inward from the burning shell $r = R_s$ and will be a good description of the structure as long as the electrons remain nondegenerate and the mass of the region is negligible in comparison to that of the core ($\Delta m(r) \ll M_c$). As ρ_s is, in most cases, much lower than the mean density of the core ($\rho_s \ll \bar{\rho}_c$), Equation (42) can be integrated quite far from the burning shell ($|r - R_s| \lesssim R_s$) and still fulfill $\Delta m(r) \ll M_c$. Integrating the density inward we find that in the (almost) massless mantle below the burning shell, the density follows

$$\rho(r) = \rho_- e^{\frac{G\mu_c M_c}{\mathfrak{R}T_-} \left(\frac{R_s - r}{R_s r} \right)}. \quad (43)$$

Equation (43) is valid as long as $\Delta m(r) \ll M_c$, and when $\rho_s \ll \bar{\rho}_c$ this equation will be valid far from the burning shell $|r - R_s| \lesssim R_s$.

A cold core supported by fully degenerate nonrelativistic electrons is described by Equation (40). However, due to Equation (43) the density drops exponentially between the degenerate core and the burning shell. The point at which the core stops to behave as a degenerate electron gas corresponds to the point at which the pressure from the nondegenerate ion gas starts to be more important than that of the degenerate electrons. The density at the boundary of the degenerate core

¹⁵ Otherwise a flash would develop, injecting huge amounts of energy in that layer, and lifting degeneracy.

¹⁶ This mantle is clearly seen in detailed stellar models; see Appendix A.

(ρ_{Bdc}) can be estimated by setting $P_{e^-} = P_{\text{ions}}$,¹⁷

$$\rho_{\text{Bdc}} \approx 1.7 \times 10^{-8} T_s^{3/2} [\text{cgs}], \quad (44)$$

where we have used that in the absence of neutrino cooling the degenerate core behaves isothermally due to the high heat transport efficiency of degenerate electrons. Note that for typical H-burning temperatures the density at the boundary of the degenerate core $\rho_{\text{Bdc}} \ll \langle \rho_{\text{dc}} \rangle = 3M_{\text{dc}}/(4\pi R_{\text{dc}}^3)$, which means that ρ_{Bdc} is almost zero in comparison with $\langle \rho_{\text{dc}} \rangle$, and its location can be approximated by radius of the $n = 3/2$ polytrope (Equation (40)). The condition $\rho_{\text{Bdc}} \ll \langle \rho_{\text{dc}} \rangle$ also implies that Equation (43) is valid for values of $|r - R_s| \gtrsim R_s$, and the inner mantle can be treated as massless; $M_{\text{dc}} \simeq M_c$. In particular, if we now integrate the inner mantle (Equation (43)) down to the location of the upper boundary of the degenerate core, we get

$$1.7 \times 10^{-8} T_s^{3/2} \approx \rho_{\text{Bdc}} \approx \rho_e e^{\frac{G\mu_c M_c}{9kT_s} \left(\frac{R_s - R_{\text{dc}}}{R_s R_{\text{dc}}} \right)}. \quad (45)$$

Equation (45) gives a new relation between ρ_s , T_s , and M_c and R_s . This relation must be fulfilled together with those coming from Equations (36), and (23). Note in passing that each of these equations represents a relation imposed by the three distinctive regions of our star: the core (Equation (45)), the burning shell (Equation (36)), and the envelope (Equations (29) and (23)).

3.2. A Complete Toy

Before continuing with our analysis we will write Equation (45) in a more favorable way. Replacing Equation (23) into Equation (45), and using $\nabla_+ \simeq (a+1)/(4-b)$ we can write

$$\begin{aligned} \rho_s &\simeq 5.33 \times 10^5 \frac{\mu_s}{\mu_c} \exp\left(-\frac{1}{\nu} \frac{(7-2b-a)}{(a+1)}\right) (1+1/\nu)^{3/2} \\ T_9^{3/2} &\exp\left(\frac{(4-b)}{(a+1)} \frac{1}{(1+2/\nu)} \frac{\mu_c}{\mu_{\text{env}}} \left(1 - \frac{R_{\text{dc}}}{R_s}\right)\right). \end{aligned} \quad (46)$$

At the densities and temperatures typical of the burning shell and the upper mantle, the opacity is dominated by electron scattering,¹⁸ and can be approximated as

$$\kappa_e = 0.2(1+X)\text{cm}^2/\text{g}. \quad (47)$$

At the burning shell (hydrogen mass fraction $X \sim 0.35$) we have $\kappa_s \simeq 0.27\text{cm}^2/\text{g}$. The energy generation due to CNO burning in that temperature range, $T_s/10^9 = T_9 \in (0.001, 0.1)$,

¹⁷ Note that it is reasonable to assume that electrons are degenerate in this estimation as the density at which electrons stop to behave as a degenerate gas corresponds to $\epsilon_{\text{Fermi}} \approx kT$, which corresponds to

$$\rho(\epsilon_{\text{Fermi}} \approx kT) \approx 1.2 \times 10^{-8} T^{3/2},$$

which is lower than the density in Equation (44).

¹⁸ While the core is below $M_c \lesssim 0.23M_\odot$ and the shell temperature is close to $\sim 3 \times 10^7\text{K}$, Thomson scattering is not the only relevant source of opacity, and other sources, mostly bound-free opacities are also important. It is only after $M_c \sim 0.25M_\odot$ that Thomson scattering becomes dominant at the shell temperature. In Appendix B we show that qualitative behavior is unaltered when a Kramers' bound-free opacity law is adopted.

is well approximated by

$$\epsilon_{\text{CNO}} \simeq 8.24 \times 10^{25} X_{\text{CNO}} X_{\rho_s} T_9^{-2/3} \exp(-15.231 T_9^{-1/3}), \quad (48)$$

where for a typical composition we have $X_{\text{CNO}} \simeq 0.01$. The choice of Thomson scattering and CNO burning corresponds to $a = b = 0$ and $t = 1$ in the expressions of ϵ and κ , as discussed in Section 2. The temperature dependence ν of the nuclear generation rate is,

$$\nu = \frac{d \ln \epsilon_{\text{CNO}}}{d \ln T_9} \simeq \left(-\frac{2}{3} + 5.077 T_9^{-1/3}\right). \quad (49)$$

This expression gives $\nu \simeq 23, 13$ and 10 for $T_9 \simeq 0.01, 0.05$, and 0.1 respectively, as it should.

In these conditions, Equation (39) becomes

$$\begin{aligned} \left(\frac{\mu_s}{\mu_{\text{env}}}\right)^2 &\simeq 5.099 \\ &\times 10^{-10} \frac{\rho_s^3 R_s^2 T_9^{-14/3}}{\nu} \exp(-15.231 T_9^{-1/3}). \end{aligned} \quad (50)$$

Replacing Equation (46) into Equation (50) we have, for the case of Thomson scattering

$$\begin{aligned} &1.2953 \times 10^{-8} \frac{\mu_c^3}{\mu_s \mu_{\text{env}}^2} \nu \exp(21/\nu) (1+1/\nu)^{-9/2} \\ &= T_9^{-1/6} R_s^2 \exp\left[\frac{12}{(1+2/\nu)} \frac{\mu_c}{\mu_{\text{env}}} \left(1 - \frac{R_s}{R_{\text{dc}}}\right) - 15.231 T_9^{-1/3}\right]. \end{aligned} \quad (51)$$

Now we can rewrite Equation (51) and Equation (23) in a more convenient way by properly normalizing R_s , leaving an explicit dependence on the mass of the core. These equations result in

$$\frac{R_s}{R_{\text{dc}}} \simeq \frac{\mu_{\text{env}}}{\mu_c} \frac{0.6}{T_9} \left(\frac{M_{\text{dc}}}{M_\odot}\right)^{4/3} \quad (52)$$

and

$$\begin{aligned} &1.633 \times 10^{-26} \frac{\mu_c^3}{\mu_s \mu_{\text{env}}^2} \nu \exp(21/\nu) (1+1/\nu)^{-9/2} \\ &= T_9^{-1/6} \left[\frac{R_s}{R_{\text{dc}}}\right]^2 \left[\frac{M_c}{M_\odot}\right]^{-2/3} \\ &\times \exp\left[\frac{12}{(1+2/\nu)} \frac{\mu_c}{\mu_{\text{env}}} \left(1 - \frac{R_s}{R_{\text{dc}}}\right) - 15.231 T_9^{-1/3}\right]. \end{aligned} \quad (53)$$

Typical values for the mean molecular weight are $\mu_c/\mu_s \simeq 1.58$, $\mu_c/\mu_{\text{env}} \simeq 2.167$. The actual value of $T_9(M_c)$ and $R_s(M_c)$ is not strongly affected by factors of order 1 on the left-hand side of Equation (53) and is dominated by the exponents in T_9 , R_s and the exponential function. In particular, we see that the exponential contains a factor μ_c/μ_{env} , which explains the well-known fact that the temperature of the burning shell, and consequently the luminosity of the shell, is affected by the molecular weight contrast between the envelope and the core. This is the reason why some previous works have found that molecular weight contrast between the envelope and the core

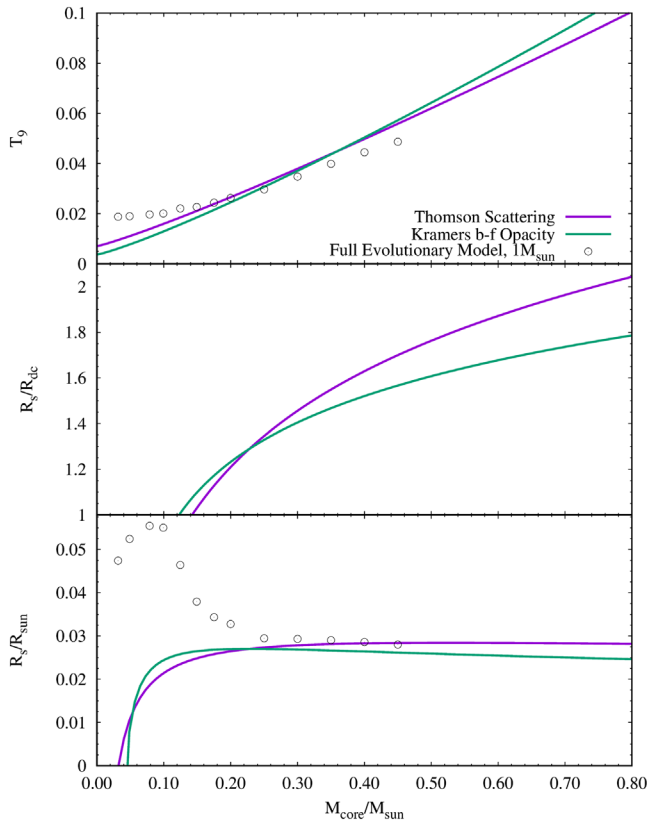


Figure 4. Values of R_s and T_9 for different core masses that fulfill Equations (52) and (53) and the corresponding equations for Kramers’ bound-free opacities; see Appendix B.

helps the development of the giant structure (Stancliffe et al. 2009). In addition, these expressions show us that estimating the impact of the molecular weight on the luminosity of the shell by means of shell homology relations where one considers the changes in μ and R_c as independent is not completely right (see Chapter 33.2 in Kippenhahn et al. 2012). In a full stellar model altering the molecular weight of the envelope will have an impact on the radius of the burning shell, which also alters the temperature of the shell.

By replacing $T_9(R_s)$ or $R_s(T_9)$ from Equation (52) into Equation (53) we obtain the solutions for $T_9(M_c)$ and $R_s(M_c)$. These solutions are shown in Figure 4, and can be very well approximated by

$$T_9 = 0.0071 + 0.12 \left(\frac{M_c}{M_\odot} \right)^{1.13}$$

$$\frac{R_s}{R_{dc}} = 2.181 + 0.589 \ln \left(\frac{M_c}{M_\odot} - 0.008 \right). \quad (54)$$

Similar expressions for a Kramers’ opacity are derived in Appendix B. Figure 4 shows the predicted evolution of the temperature and radius of the H-burning shell as the mass of the core increases as a consequence of nuclear burning in our toy model. The resulting density of the burning shell is shown in Figure 5.

We see that the burning shell settles near the degenerate core but moves away from it as the shell becomes hotter. As a consequence the burning shell settles at an almost constant

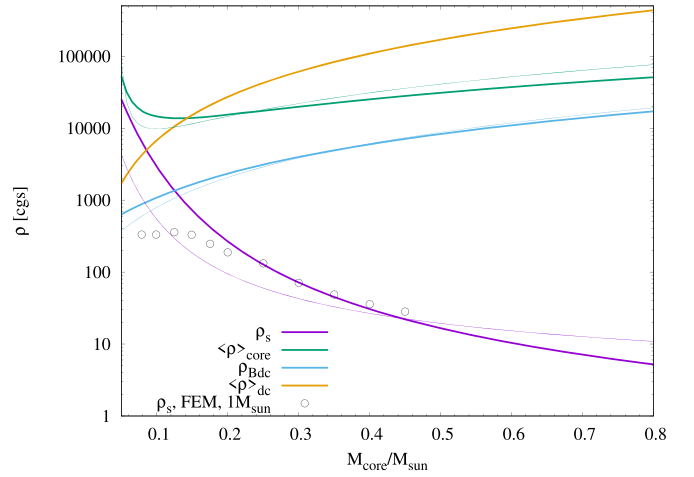


Figure 5. Dependence of the density of the shell as a function of the mass of the core compared with other key densities of our toy model. Thick lines indicate the relations obtained for Thomson scattering, while thin lines depict the same relations for a Kramers’ bound-free opacity.

value of $R_s \simeq 0.026$ (middle and lower panels in Figure 4). The fact that our toy model is able to reproduce the radius of the burning shell predicted by the full stellar evolution model to less than 10% is a remarkable confirmation of the validity of our assumptions. We now see that the constancy in the radius of the burning shell is the consequence of the existence of an ideal gas mantle on top of a degenerate core. As the mass of the core increases, it forces a drop in the density of the burning shell. As the degenerate part of the helium core contracts (following $R_{dc} \propto M_c^{-1/3}$) the density of the isothermal mantle between the degenerate core and the burning shell drops (so that the density in this region can go from ρ_{Bdc} to ρ_s). This stretches the isothermal mantle of ideal gas, counterbalancing the mild contraction of the degenerate part of the core, and leading to an almost constant radius of the burning shell.

In spite of all simplifications in the treatment of the core and the fact that the envelope is only required to be massive enough and fulfill outer boundary conditions, the model gives a very good quantitative agreement with the temperature and radius of the shell derived from the detailed computation of the full set of stellar evolution equations by means of a state-of-the-art stellar evolution code (LPCODE; Miller Bertolami 2016). This is particularly true once the thin shell approximation adopted throughout this paper becomes good and the density contrast between the shell and the core is high, but the agreement is still good even at the beginning of the shell burning stage as R_s in the simple model deviates by less than a factor 2 from the real value of R_s (see Figure 4). This level of agreement is an astonishing confirmation of the accuracy of Equations (29), (37), and (39) and the approximations $\Theta \simeq 1$, $\Pi \simeq 1$, $\zeta \simeq 1$, and $R_s \ll R_0$ on which it is based. As we mentioned at the beginning of this article, toy models are not made to be precise but to be an accurate description of the main mechanisms of a given process, so we find this level of precision remarkable.

Besides the confirmation of our key equations, our toy model offers some very interesting insight on the structure of low-mass red giants. The model shows why the existence of a mantle of negligible mass above the degenerate core increases its radius, so that, as the core increases its mass and the radius of the degenerate regions decrease as $M_c^{-1/3}$, the radius of the burning shell stays at a constant value of $R_s \simeq 0.027 \dots 0.03 R_\odot$.

In addition, the model helps us understand why all low-mass stars develop a He flash when the core mass is about half a solar mass irrespective of the initial mass, metallicity, or mass of the envelope. We see that, for a star with a completely isothermal and thermally relaxed core, the H-burning shell (and consequently the core) reaches He-burning temperatures when the mass of the core is $M_c \simeq 0.75M_\odot$, independent of the metallicity and the mass of the envelope. This sets an upper limit for the mass of the core at the moment of the He-core flash. The fact that the He flash happens before the core reaches this limiting mass is due to gravothermal heat release (see the discussion in Appendix A). As the core increases its mass and the H-burning shell heats up, the timescale of nuclear reactions becomes shorter and comparable with the thermal (Kelvin–Helmholtz) timescale of the core. This additional heating of the core anticipates the development of the He flash. However, as this additional heating is a function of the rate at which mass is added to the core (\dot{M}_c), and \dot{M}_c is solely determined by T_s , the mass of the core at which the helium flash will happen will be almost constant and irrespective of the initial mass, metallicity, and mass of the envelope.

4. Dimensional Analysis

Now that we have confirmed the accuracy of the equations derived in Section 2 we can turn to analyze their implications for the global structure of stars.

From Equation (37) we know that $T_s \propto M_c/R_s$, replacing now this into Equation (36) we find that

$$P_s = \mathcal{K} R_s^{(\nu-t-8+b)/(a+t+2)} M_c^{(6-\nu+t-b)/(a+t+2)}, \quad (55)$$

where \mathcal{K} is a constant that can be computed from Equation (36). Due to hydrostatic equilibrium we know that the mean pressure in the core is

$$\bar{P}_c \approx G M_c^2 / 8\pi R_s^4. \quad (56)$$

Equations (55) and (56) show that the action of the burning shell destroys the possibility of homologous contraction for these stars as it gives

$$\frac{P_s}{\bar{P}_c} = \mathcal{K}' R_s^{\frac{\nu+3t+b+4a}{a+t+2}} M_c^{\frac{2-\nu-t-b-2a}{a+t+2}}. \quad (57)$$

In fact as ν is the dominant term in both exponents, Equation (58) tells us that, as soon as R_s contracts or M_c increases by a small amount, pressure at the burning shell drops by orders of magnitude. To quantify this point let's focus on the most common situation in both low- and high-mass red giants, Thomson scattering ($a = b = 0$) with CNO burning ($t = 1$ and $\nu \sim 23 \dots 13$). Under those conditions, Equation (58) gives

$$\frac{P_s}{\bar{P}_c} = \mathcal{K}' R_s^{1+\nu/3} M_c^{\frac{1-\nu}{3}}. \quad (58)$$

For typical values of ν , $(1 + \nu/3) \sim 8.5 \dots 5.3$, then a small decrease in the radius of $\sim 10\%$ leads to a $\sim 50 \dots 80\%$ drop in the ratio between the pressure at the shell and that at the core. This is the situation in massive and intermediate-mass stars (IM&M), where the location of the shell decreases by at least a factor of 2, between the end of core H burning and the beginning of He burning, while the mass of the core remains constant, leading to a huge drop of more than 2 orders of magnitude in P_s/\bar{P}_c . Note in passing that for IM&M stars \dot{r}

does not change sign at the maximum of their energy release, as stated by Kippenhahn et al. (2012), but immediately above the burning shell in the region where the density drops many orders of magnitude. On the contrary, in low-mass stars, as we have seen in the previous section the interplay between the inner mantle and the degenerate part of the core renders the position of the shell almost constant (i.e., $\dot{r} = 0$) while the mass of the core increases.

Using Equation (37) and the equation of state we can also obtain

$$\rho_s = K'' R_s^{(\nu-6+b+a)/(a+t+2)} M_c^{(4-\nu-a-b)/(a+t+2)}. \quad (59)$$

A knowledgeable reader will recognize the exponents in Equations (55), (58), and (59) as those provided by shell homology relations. This should come as no surprise as in Section 2.5 we mathematically demonstrated that to this level of approximation the key hypothesis of shell homology relations is rigorously valid (i.e., that $T_s(M_c, R_s)$, $\rho_s(M_c, R_s)$, and $P_s(M_c, R_s)$). Consequently, any dimensional analysis based on our relations should cast the same result. The main difference between Equations (55) and (59) and those derived by shell homology relations is that here we are able to compute (if required) the numerical values of the proportionality constants \mathcal{K} , \mathcal{K}' , and K'' .

5. A Red Giants' Toy Story

We are now in condition to qualitatively understand the development of red giant structures after the main sequence. The existence of an envelope of nonnegligible mass forces the mean value of $\nabla \simeq 0.23\text{--}0.4$ above the burning shell, which leads to a tight dependence of the shell temperature on the mass and radius of the core $T_s \propto M_c/R_s$ (Equation (23)). Additionally, the switching-on of the burning shell and the fact that the heat is both generated and transported at the burning shell leads to a tight relationship between ρ_s , T_s , M_c , and R_s (Equation (36)). Together, Equations (23) and (36) imply that $\rho_s(M_c, R_s)$. For a given mass–radius relation of the core, $M_c(R_s)$ this implies that the shell density will evolve as a function of M_c or R_s . Below we will analyze the typical mass–radius relations for low-mass stars and IM&M stars. Interestingly we will see that these two cases correspond quite well with evolutions at constant R_s or M_c , respectively.

The situation is simpler in more massive stars, where the core is an undifferentiated contracting sphere with the same equation of state, while it is more complicated for low-mass stars where the core can be divided into a degenerate core and a surrounding mantle that behaves as an ideal classical gas. In the latter case we will make use of the simple $R_s(M_c)$ relation derived in Section 3.

5.1. Low-mass Stars

As soon as H burning is exhausted in the core the layers around it start to contract and heat up as a consequence of the negative gravothermal specific heat of typical of nondegenerate stellar material¹⁹, leading to the ignition of a H-burning shell around the exhausted core.

¹⁹ In stars with masses between $1.1M_\odot \lesssim M_* \lesssim 2M_\odot$ the former convective core first contracts in a Kelvin–Helmholtz timescale until the layers surrounding the He core reach H-burning temperatures. On the contrary, in lower-mass stars $M_* \lesssim 1.1M_\odot$ the transition from core H burning to shell H burning happens continuously.

The formation of a degenerate core surrounded by a hot mantle (Section 3.2) leads to stringent mass–radius relation for the core. Together with the constraints coming from the massive envelope and the burning shell (Equations (23) and (36)) this forces the radius of the burning shell to settle at a very specific constant location and at specific values of temperature and density, all of which are solely defined by the mass of the core below the burning shell (Equation (54) and Figures 4 and 5). As M_c only increases due to the H consumption at the burning shell, $T_s(M_c)$, $\rho_s(M_c)$, $P_s(M_c)$, $R_s(M_c)$ will evolve on a nuclear timescale. For low-mass red giants (Equation (54)) R_s is forced to remain almost constant, and we get $P_s/\bar{P}_c \propto M_c^{(2-\nu-t-b-2a)/(a+t+2)}$ and $\rho_s/\bar{\rho}_c \propto M_c^{(2-\nu-2a-b-t)/(a+t+2)}$. At first the switching-on of the H-burning shell does not lead to a particularly increase in the geometrical size of the star, because for low core masses $M_c \lesssim 0.12M_\odot$ the density of the shell does not differ so much from that of the core, which means that similar amounts of mass are harbored in similar volumes both in the core and around the burning shell (Figure 5). However, as the mass of the core increases due to nuclear burning, the density of the shell and the density of the core evolve in opposite directions and soon much larger volumes are needed to harbor masses around the burning shell. In our toy homogeneous model already at $M_c \approx 0.12M_\odot$ the density of the shell is about 1 order of magnitude lower than the mean density of the core $\bar{\rho}_c$. The drop in density of the shell leads to a drop in the density of the envelope leading to an increase in size. This situation is made extreme by the enforcement of hydrostatic equilibrium on the upper mantle as we will show in the next paragraph.

Equation (24) is valid as long as $m(r) \simeq M_c$. Let us define a point R_{BAP} , which sets the boundary of the validity for the massless approximation, i.e., $(m(R_{\text{BAP}}) - M_c) = Q M_c$ with $Q \ll 1$. For example, with $Q = 0.1$ our estimations of T , ρ in that mantle will be wrong by less than 10%. Within that upper mantle density drops as

$$\rho(r) \approx \rho_s \left(\frac{r}{R_s} \right)^{-\delta}, \quad (60)$$

with $\delta = (3 - b - a)/(a + 1)$. For the usual situation of Thomson Scattering $\delta = 3$. Integrating the mass up to R_{BAP} we have

$$\Delta M = Q M_c = \rho_s \int_{R_s}^{R_{\text{BAP}}} 4\pi r^2 \left(\frac{r}{R_s} \right)^{-\delta} r^2 dr. \quad (61)$$

Solving the integral and using the definition of $\bar{\rho}_c$ we find that, for $\delta = 3$

$$R_{\text{BAP}} = R_s \exp \left(\frac{Q \bar{\rho}_c}{3 \rho_s} \right), \quad (62)$$

which is a remarkable result. Equation (62) shows that as soon as the density contrast between the core and the shell increases the radius of the *massless* upper mantle on top of the shell increases exponentially. This is a very well-known feature of numerical models. The situation is even more extreme for bound-free opacities $\delta = 3.5$, and the density drops faster.

The direct consequence of this drop in the density contrast is that the boundary of the massless mantle is moved far away from the core ($R_{\text{BAP}} \gg R_s$), and the density of the material drops orders of magnitude to

$$\rho_{\text{BAP}} = \rho_s \exp \left(\frac{Q \bar{\rho}_c}{3 \rho_s} \right)^{-\delta}, \quad (63)$$

while the pressure drops as

$$P_{\text{BAP}} = P_s \exp \left(\frac{Q \bar{\rho}_c}{3 \rho_s} \right)^{-(1+\delta)}. \quad (64)$$

As pointed out by Faulkner (2005), the star is then left with the daunting task of harboring the whole massive envelope with a very low density and under a very low gravitational potential (due to the large increase in R_{BAP}). A simple estimation from the hydrostatic equilibrium equation (setting $P_{\text{surface}} \approx 0$) gives

$$\bar{R}_{\text{env}} \simeq \frac{(G/4\pi)^{1/4} (M_c M_{\text{env}})}{P_{\text{BAP}}^{1/4}}, \quad (65)$$

and the exponential drop in P_{BAP} leads to a large increase in the value of the typical radius \bar{R}_{env} of the mass shells in the massive envelope. Note that this qualitative conclusion is valid regardless of whether the massive envelope is radiative or convective.²⁰

Note that while ρ_s stays within 1 order of magnitude of $\bar{\rho}_c$, the exponent $(Q \bar{\rho}_c)/(\rho_s 3)$ is close to unity and nothing happens. In our toy model (Figure 5) this corresponds to $M_c \lesssim 0.1M_\odot$ (depending on the exact value of Q adopted). We see that our simple model predicts that the change in the behavior of the radius of low-mass red giants should appear once $M_c \gtrsim 0.1M_\odot$, but not before. Figure 6 shows the behavior of the stellar radius as a function of the mass of the core for $1M_\odot$ and $1.8M_\odot$ full evolutionary models computed with LPCODE. It is clear from Figure 6 that there is a change in the behavior of the radius as a function of the mass of the core at $M_c \sim 0.125M_\odot$. This is particularly easy to see in the case of the $1M_\odot$ model, in which H burned in the core radiatively and thus had a smooth transition to shell burning. Stellar models with cores smaller than this threshold change their radii by less than a factor of 2 even with an increase in the mass of the core of more than 1 order of magnitude.

5.2. Intermediate-mass and Massive Stars (IM&M)

The situation in IM&M stars is fortunately much simpler than that of low-mass stars. This is because their core is not differentiated and can be modeled as a contracting sphere of ideal gas. For stars in this mass range, the mass of the exhausted core after the main sequence is larger²¹ than the Schönberg–Chandrasekhar limit, and the exhausted core contracts on a thermal timescale. As this timescale is shorter than the nuclear timescale at which the burning shell adds mass to the core, the evolution will proceed at almost constant M_c . As soon as core H burning is finished and as temperatures around the burning shell reach $T \sim 10^7 K$, we can estimate the mean pressure in the core to be

$$\bar{P}_c \approx \frac{GM_c^2}{8\pi R_s^4} + P_s, \quad (66)$$

²⁰ It is affected, however, by very deep convection so that convection reaches down to the burning shell itself. In fact, very deep convection is known to reduce the size of red giant stars; see Appendix C.

²¹ For stars below $\approx 3M_\odot$ this limit is reached later after enough fresh He has been added to the core by the burning shell; see Salaris & Cassisi (2005).

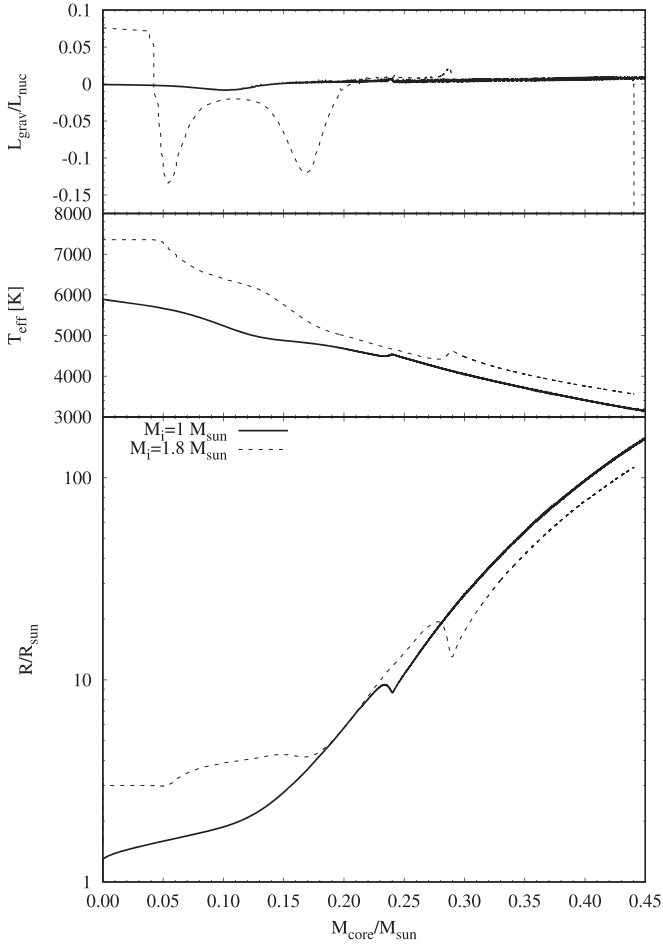


Figure 6. Evolution of the radius of a $1M_{\odot}$ model ($Z = 0.02$) as a function of the mass of the He core.

and the mean density of the core is

$$\bar{\rho}_c \approx \frac{3M_c}{4\pi R_s^3}. \quad (67)$$

As the equation of state in the contracting cores of massive and intermediate-mass stars corresponds to that of a classical ideal gas, we know that typical temperatures in the core are

$$\bar{T}_c \approx \frac{\mu \bar{P}_c}{\mathfrak{R} \bar{\rho}_c}. \quad (68)$$

The evolution of those cores is ruled by the speed at which they lose energy from their surface, as $L_c \neq 0$. The Virial theorem for such structures tell us that

$$2E_i + E_g = 4\pi R_s^3 P_s. \quad (69)$$

Using the expression for the internal energy of an ideal monoatomic gas and for the gravitational energy we find that

$$k' \frac{3M_c \mathfrak{R} \bar{T}_c}{\mu_c} - \frac{kGM_c^2}{R_c} = 4\pi R_s^3 P_s, \quad (70)$$

where k' and k are form factors of the order of unity that depend on the details of the mass distribution of the core. In the most representative case of Thomson scattering, P_s can be replaced

as a function of M_c and R_s to give:

$$k' \frac{3\mathfrak{R} \bar{T}_c}{\mu_c} = \frac{kGM_c}{R_c} + 4\pi k'' R_s^{\nu/3} M^{(4-\nu)/3}. \quad (71)$$

The time evolution of the core of massive stars is given by $-d(E_i + E_g)/dt = L_c$, and consequently $L_c = dE_i/dt = -(dE_g/dt)/2$. As heat is radiated away from the core ($L_c > 0$) at constant mass²², the temperature will rise and the radius will shrink. Due to the large value of ν , the surface terms in Equations (71) and (66) become quickly irrelevant. As contraction proceeds at constant mass we see that

$$\frac{\rho_s}{\bar{\rho}_c} \propto R_s^{1+\nu/3},$$

$$\frac{P_s}{\bar{P}_c} \propto R_s^{1+\nu/3}, \quad (72)$$

$$\frac{T_s}{\bar{T}_c} \propto R_s^0 = 1. \quad (73)$$

Due to the large exponents we see that the contrasts in the density and pressure increase very rapidly with moderate contractions of the core. Again, as in the case of low-mass stars, the development of a large density contrast has enormous consequences for the hydrostatic equilibrium of the upper mantle on top of the burning shell. In fact, the derivations of Equations (62), (63), (64), and (65) done in Section 5.1 are independent from the specific characteristics of the core and are valid also when the stellar core corresponds to an ideal classical gas. A small contraction of the core leads to an increase in the density contrast of the star and, as before, this will lead to a further drop in the pressure and density (P_{BAP} , ρ_{BAP}) and an increase in the radius (R_{BAP}) at the bottom of the massive envelope. The envelope of mass M_{env} has to be accommodated in a very low gravitational potential and with very low densities, which causes a huge increase in the typical radius (R_{env}) of its layers.

Note that although the shell remains at an almost constant location in the case of low-mass stars, this is not true for IM&M stars (see Figure 7). Due to the different central temperatures at the end of the main sequence ($T/10^7 = 3.6, 4.3, \text{ and } 5.8$ at the end of the main sequence for the $3 M_{\odot}, 5 M_{\odot}, \text{ and } 10 M_{\odot}$ models), different degrees of core contraction are required before helium-burning temperatures are attained ($T_c \sim M_c/R_s$). For example, in the sequences shown in Figure 7 between the end of the main sequence and the beginning of He burning, the core contracts by $R_s^0/R_s \simeq 2.5, 2.2, \text{ and } 1.9$ for the $3 M_{\odot}, 5 M_{\odot}, \text{ and } 10 M_{\odot}$ sequences. These changes in R_s correspond to increases in the density of $\bar{\rho}_c/\bar{\rho}_c^0 \simeq 15.6, 10.6, \text{ and } 6.8$.

6. Conclusions and Final Remarks

In this work we have revisited the long standing question of why stars become red giants by means of a detailed analysis of the stellar structure equations. Contrary to the suggestions by Iben (1993) and Whitworth (1989), we find that a simple analytic answer is possible. Our analysis is inspired by the physical insight offered by Faulkner (2005), but it is based on a

²² Because contraction happens on timescales much shorter than those of nuclear reactions.

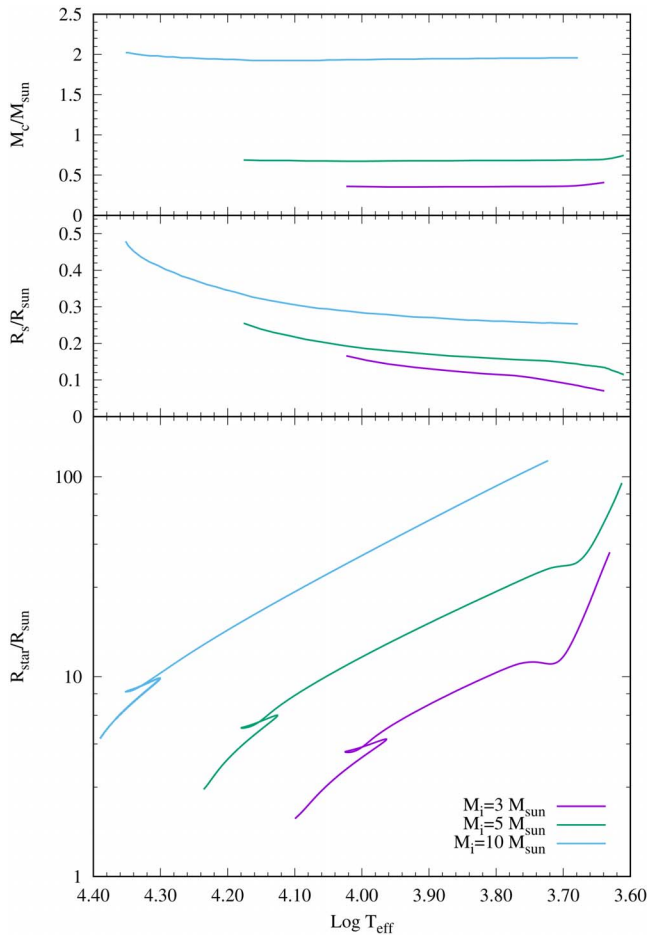


Figure 7. Evolution of the core mass M_c , shell radius R_s , and stellar radius of three full evolutionary sequences with initial masses $3 M_\odot$, $5 M_\odot$, and $10 M_\odot$ ($Z = 0.02$).

more solid logical and mathematical derivation, offering deeper insight into the structure of red giants. Most importantly, our analysis done in Section 2.1 highlights the role played by convection in the development of (bright) red giants. Contrary to the conclusion of Faulkner (2005), that convection only acts to make stars smaller (see item (e) in Appendix 10.A.2 of Faulkner 2005), we find that the development of convection is a key ingredient. It is the development of convection what sets the upper boundary to the value of ∇_+ , leading to the existence of the $T_s(M_c, R_s)$ relation. This fact explains why earlier models in which convection was neglected did not become luminous red giants—see for example Figure 3 in Sandage & Schwarzschild (1952) but also Figure 2 of Stancliffe et al. (2009). The fact that Faulkner (2005) is able to derive a core mass–luminosity relation (his Equation 10.7) with no mentioning of the role of convection highlights the problem with the mathematical derivations in that work, and in particular with the analysis done in their Appendix 10.A.2.

Our findings can be summarized as follows. The existence of an envelope of nonnegligible mass forces ∇ to have a very narrow range of possible values ($0.23 \lesssim \nabla \leq 0.4$, for typical opacity laws), which leads to a tight dependence of the shell temperature on the mass and radius of the core $T_s \propto M_c/R_s$ (Equation (23)). Additionally, the switching-on of the burning shell and the fact that the heat is both generated and transported at the burning shell leads to a tight relationship between ρ_s , T_s ,

M_c , and R_s (Equation (36)). Together, Equations (23) and (36) imply that $\rho_s(M_c, R_s)$ (and consequently $P_s(M_c, R_s)$). In a full stellar structure, these constraints are then complemented by mass–radius relations for the core $M_c(R_s)$. The addition of this restriction leads to unique values for T_s , ρ_s , and P_s as a function of either R_s or M_c . This forces a very different evolution for ρ_s and P_s as a function of either R_s or M_c in comparison to their core counterparts \bar{P}_c and $\bar{\rho}_c$, making homologous contraction impossible.

Although the $M_c(R_s)$ relation of the cores is different in low-mass stars and in intermediate-mass and massive (IM&M) stars, the consequences are the same. In low-mass stars the combination of a degenerate massive inner region and a massless hot mantle below the burning shell leads to an almost constant value of R_s , while the mass of the core increases as nuclear burning consumes the H envelope. On the contrary, on IM&M stars the Kelvin–Helmholtz contraction of the classical ideal gas in the core leads to the decrease in the radius of the core but at almost constant mass. In both low-mass and IM&M stars, however, evolution leads to an increase in the mean pressure \bar{P}_c and density $\bar{\rho}_c$ of the core. Most importantly, evolution in both low-mass and IM&M stars leads to an increase in the pressure and density contrasts between the shell and the core (\bar{P}_c/P_s and $\bar{\rho}_c/\rho_s$). This increase in $\bar{\rho}_c/\rho_s$ leads to a huge expansion of the mantle on top of the burning shell, where both the pressure and density drop by orders of magnitude. The massive envelope on top of this mantle is then forced to very low densities and low gravitational potentials, leading to very large stellar radii. The storage of a massive envelope at low densities leads to the formation of a red giant.

Besides finding a toy-model description for the formation of red giants some additional findings of the present work are worth mentioning. First, the $T_s(M_c, R_s)$, $\rho_s(M_c, R_s)$, and $P_s(M_c, R_s)$ relations derived from the analysis of the burning shell (and the lower envelope) are, to the best of our knowledge, the first mathematical demonstration of this key hypothesis behind shell homology relations (Kippenhahn et al. 2012). Second, while it is known since the work of Hayashi (1947) that stellar models become giants even when convection is suppressed, our simple model shows that convection plays a key role in the formation of the actual luminous red giants that we observe. Next, it is clear from the current presentation why a molecular weight gradient helps the development of a giant structure, although it is neither a sufficient nor a necessary condition (Stancliffe et al. 2009). The development of a weight gradient between the core and the shell helps increase the density contrast $\bar{\rho}_c/\rho_s$ between the core and the envelope, but it is not the only way to attain a large density contrast. In addition, our toy model shows that it is not completely correct to estimate changes in the luminosity of the shell due to changes in the molecular weight without including the feedback of this change on the radius of the shell (e.g., Kippenhahn et al. 2012). Finally, our simple toy model of a low-mass red giant offers the first simple explanation of why all low-mass stars develop a He-core flash at basically the same core mass, and why this mass is of the order of $0.5 M_\odot$. In a star with an inert degenerate core the temperature of the shell solely depends on the mass of the core. In particular, this temperature reaches He-burning luminosities at $M_c \sim 0.75 M_\odot$, independently of the initial mass or metallicity. This sets a clear maximum value for the mass of the He core at the He flash. The helium flash develops well before this point because, for the high temperatures of the burning shell, the nuclear timescales

became comparable to the timescale for gravitational contraction. As a consequence, gravitational contraction provides an additional heating source, leading to an advance of the He flash. Interestingly, as this advance is a consequence of the rate of growth of the degenerate core, and that rate ($dM_c/dt \propto L_s$) solely depends on the mass of the core, the helium flash is advanced by the same amount in all low-mass stars.

From a pedagogical perspective, we believe that having a simple physical model to explain how stars become luminous red giants will improve our teaching of stellar evolution, and also our interpretation of results from detailed numerical models. In future works we will apply the model presented here to the explanation of other properties of stellar models like the red giant bump (Christensen-Dalsgaard 2015; Hekker et al. 2020) or the critical mass at which stars depart from the red giant branch (Soker 2008).

In closing let us mention that, given the past history of this topic, we do not expect this paper to end the discussion on the subject. We hope, however, that the ideas presented in this paper might offer a different perspective for future discussions.

M3B warmly thanks Jørgen Christensen-Dalsgaard, Achim Weiß, Tiara Battich, Santi Cassisi, Leandro G. Althaus, Alfred Gautschy, and the two anonymous referees for their comments and criticism on different versions of the manuscript that helped improve and correct the paper. Jørgen Christensen-Dalsgaard and Achim Weiß are particularly acknowledged, the former for his very detailed feedback and encouragement, and the latter for his patience with the author during the many discussions about this topic in the last 15 yr. Tiara Battich is also acknowledged for her continuous support during the realization of this work. M3B is partially supported by PIP 2971 from CONICET and PICT 2020-03316 from Agencia I +D+i. The author thanks the Max Planck Institute for Astrophysics without whose library this research would have been impossible. The author also thanks I. Newton for the idea of what to do during a pandemic lockdown. Finally, M3B is especially grateful to the editor (Dr. Steven Kawaler) for his patience and positive approach to the peer review process. This work is dedicated to Mabel A. Bertolami who taught the author the values of hard work and perseverance, which were key for the successful realization of this work.

Software: LPCODE: Miller Bertolami (2016).

Appendix A

The Inner and Upper Mantle in Detailed Numerical Models

In this section we show the main structural properties of the core, shell, and upper mantle in a detailed numerical simulation of a $1M_\odot$, $Z = 0.02$ star on the red giant branch. We do this for the sake of completeness and also to show the reasons behind the identification of the main parts of a low-mass red giant (Figure 3). Figure 8 shows the temperature and density structure of a detailed $1M_\odot$ model as it evolves on the red giant branch.

The existence of the inner isothermal mantle is apparent in all models right below the burning shell (upper panel of Figure 8). As expected from the discussion in our toy model, in this region the density drops exponentially with increasing radius, from the typical values in the degenerate core down to the density of the burning shell (lower panel of Figure 8). Note that, although extended in radius, the upper mantle region shown in Figure 8 harbors a negligible amount of mass, due to

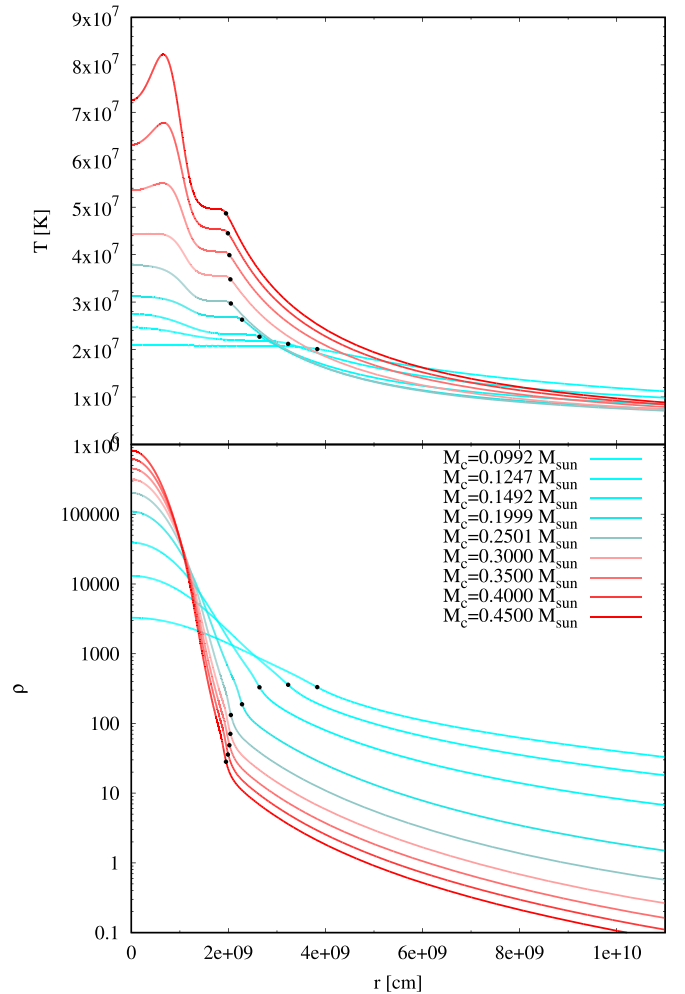


Figure 8. Density and temperature profiles of the $1M_\odot$ model ($Z = 0.02$) for different core masses. Black dots indicate the location of the peak of the H-burning shell of each model.

its low densities in comparison to the core. This is clearly appreciated in Figure 9 where the properties of the models are shown as a function of the Lagrangian coordinate $m(r) = \int_0^r 4\pi r'^2 \rho dr'$. In this figure it is clear that, as soon as the star develops a relatively dense core with a significant mass ($M_c \gtrsim 0.2M_\odot$), the density drops orders of magnitude in a region of negligible mass above the burning shell (our so-called upper mantle), as a consequence of Equation (35).

A selected sample of the properties of the models at different stages of the evolution is shown in Table 1.

A clear distinction between our toy model and the actual solution of the detailed models is the fact that the cores of red giants are clearly not isothermal for two different reasons. On the one hand the material is not completely degenerate ($T = 0$) as it is still too hot for that approximation in the outermost regions of the degenerate core, and on the other hand the existence of neutrino emission leads to a decrease in the temperature of the core close to the center. Figure 10 shows a full evolutionary model near the He-core flash in comparison to the corresponding structure when gravothermal energy release is relaxed to zero (for the same chemical structure). Clearly, in thermal equilibrium the degenerate core attains a temperature almost equal to that of the burning shell, with a slight decrease

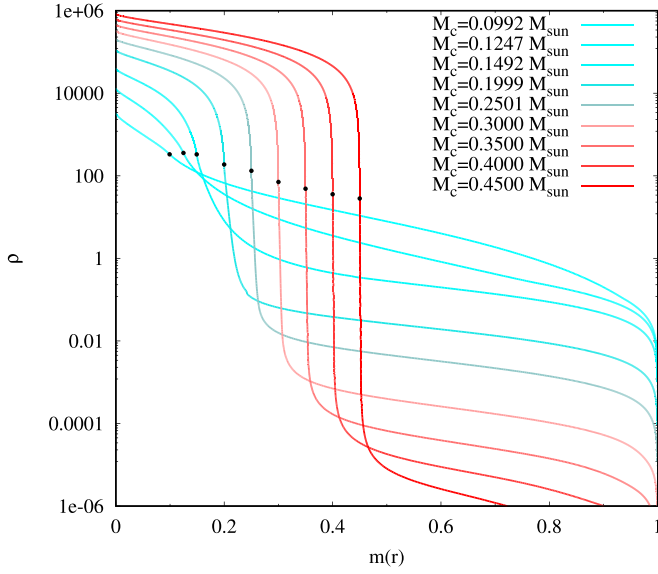


Figure 9. Density profiles of the $1M_{\odot}$ model ($Z = 0.02$) as a function of the Lagrangian coordinate $m(r)$. Black dots indicate the location of the peak of the H-burning shell of each model.

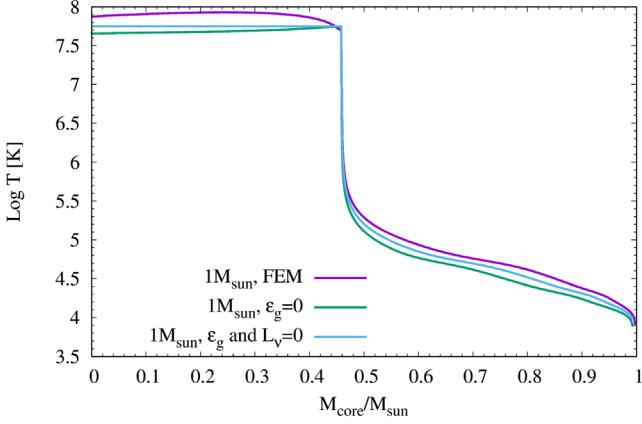


Figure 10. Temperature stratification of the $1M_{\odot}$ full evolutionary model (FEM) near the He flash. Green and cyan lines indicate the corresponding temperature stratification when the same chemical structure is fixed and the gravothermal energy release is relaxed to zero $\epsilon_g = 0$ (green), and when in addition to setting $\epsilon_g = 0$ neutrino energy losses are also set to zero.

Table 1

Properties of the Shell and the Star for Selected Snapshots in the Evolution of the $1M_{\odot}$ ($Z = 0.02$) Sequence

M_c (M_{\odot})	R_c (10^9 cm)	T_s (10^7 K)	ρ_s (g/cm^3)	R_* (R_{\odot})	$\log L/L_{\odot}$
0.0317	3.30	1.88	314*	1.286	0.256
0.0489	3.65	1.90	318	1.367	0.295
0.0788	3.86	1.97	332	1.519	0.355
0.0992	3.83	2.01	332	1.646	0.380
0.1247	3.23	2.12	358	1.916	0.378
0.1492	2.64	2.27	330	2.543	0.528
0.1752	2.39	2.44	247	3.722	0.826
0.1999	2.28	2.63	188	5.574	1.133
0.2501	2.05	2.97	132	10.51	1.593
0.3000	2.04	3.48	70.9	26.17	2.222
0.3500	2.02	3.99	48.7	53.87	2.698
0.4000	1.99	4.45	35.8	96.72	3.059
0.4500	1.95	4.87	28.2	156.5	3.336

near the center of the core, due to neutrino energy losses. If neutrino losses are also removed, then the core becomes completely isothermal (Figure 10). Figure 10 shows that the He flash happens for a lower core mass than it would were it the case that nuclear reactions had a much larger timescale than the Kelvin–Helmholtz timescale of the core.

Appendix B

Relations for a Kramers’ Bound-free Opacity Law

In Section 2 we derived the equations for the upper mantle under the assumption that opacity near the burning shell is dominated by classical electron scattering. While this is true once $M_c \gtrsim 0.23M_{\odot}$ (for a $1M_{\odot}$ star), below that core mass (and the consequent shell temperature) other sources of opacity, mostly bound-free opacities, are important. To explore the impact of this assumption we rederive the equations used in Sections 2 and 5 when Kramers’ bound-free opacity is adopted.

A very rough approximation to bound-free opacities in stellar interiors is provided by Hansen et al. (2004), which for a typical composition of the envelope ($X = 0.7$, $Z = 0.02$) is (in cgs)

$$\kappa_{b-f} = 4.3 \times 10^{-8} \rho T_9^{-7/2}. \quad (\text{B1})$$

With this new opacity law we have $a = 1$ and $b = -4.5$, and Equations (28) and (33) can be derived in exactly the same way as before. Using these equations and the opacity law in Equation (B1) we can now derive $R_s(M_c)$ and $T_9(R_s)$ relation similar to Equations (52) and (53). These new relations are

$$\frac{R_s}{R_{dc}} \simeq \frac{\mu_{\text{env}}}{\mu_c} \frac{0.56}{T_9} \left(\frac{M_{dc}}{M_{\odot}} \right)^{4/3}, \quad (\text{B2})$$

and

$$\begin{aligned} & 1.90 \times 10^{-25} \frac{\mu_c^4}{\mu_s^2 \mu_{\text{env}}^2} \nu \exp(30/\nu) (1 + 1/\nu)^{-6} \\ &= T_9^{-13/6} \left[\frac{R_s}{R_{dc}} \right]^2 \left[\frac{M_c}{M_{\odot}} \right]^{-2/3} \\ & \exp \left[\frac{17}{(1 + 2/\nu)} \frac{\mu_c}{\mu_{\text{env}}} \left(1 - \frac{R_s}{R_{dc}} \right) - 15.231 T_9^{-1/3} \right]. \quad (\text{B3}) \end{aligned}$$

The resulting $T_9(M_c)$ $R_s(M_c)$ are shown in Figure 4 where it is clear that they share the same key features described by Equations (52) and (53); the burning shell (and consequently the isothermal core below) attains He-burning temperature at $M_c \simeq 0.7M_{\odot}$, and the H-burning shell settles at a constant radius of $R_s \simeq 0.028R_{\odot}$, very close to that predicted by full stellar evolution models.

The main difference introduced by a Kramers’ opacity law is to increase the temperature of the shell as compared to that predicted by Thomson scattering for the more massive cores. Note, however, that as soon as the temperature of the shell increases to $T \gtrsim 3 \times 10^7$ K, electron scattering becomes the main opacity source.

For the sake of completeness let us mention that the solutions shown in Figure 4 can be very well approximated by

$$T_9 = 0.0037 + 0.136 \left(\frac{M_c}{M_\odot} \right)^{1.16}$$

$$\frac{R_s}{R_{dc}} = 1.884 + 0.357 \ln \left(\frac{M_c}{M_\odot} - 0.039 \right). \quad (\text{B4})$$

Appendix C Very Deep Convection

Key equations derived in the paper rely on the radiative nature of the burning shell. Here we analyze how expressions presented in the paper are affected by convection. Let us call L_s and L_c the luminosities of the shell and core (where $L_s \gtrsim L_c$). Let us assume now that, for some reason, convection reaches deep into the burning shell to a point where the luminosity is $L_\chi = L_s \chi$ with $0 < \chi < 1$. At the convective boundary we have that $\nabla_{\text{ad}} = \nabla_{\text{rad}}$, and by equating the temperature gradients we have

$$\frac{dT}{dr} \Big|_\chi = -0.4 \frac{GM_c \mu}{\mathcal{R} R_s^2}. \quad (\text{C1})$$

From the energy generation and energy transport equations we can write

$$\left(\frac{dT}{dr} \Big|_\chi \right)^2 \simeq \frac{3}{8\pi ac} \frac{\rho_s^2 \kappa_s \epsilon_s}{T_s^2} \left(\frac{L_c}{L_s} + \chi \right) \mathcal{D}, \quad (\text{C2})$$

where $1 < \mathcal{D} < 2$ if convection has not reached the location of the peak of the burning shell and $1 = \mathcal{D}$ if it has. Together Equations (C1) and (C2) give

$$\left(0.4 \frac{GM_c \mu}{\mathcal{R} R_s^2} \right)^2 \frac{1}{\left(\frac{L_c}{L_s} + \chi \right)} \approx \frac{3}{8\pi ac} \frac{\rho_s^2 \kappa_s \epsilon_s}{T_s^2} \mathcal{D}. \quad (\text{C3})$$

Although the equations remain formally unchanged, it is clear that the deepening of convection inside the burning shell will have a strong impact. As convection deepens, then $\chi \rightarrow 0$ and the left- and right-hand sides of Equation (C3) are decoupled. Without this constraint all the arguments that allowed us to conclude that a red giant will be formed cannot be stated. In fact, if somehow a steady burning shell would develop in a completely convective star, that object would not develop a giant structure, as those stars are $n = 3/2$ polytropes and, as such, cannot develop a density contrast between the envelope and the core. It is clear that convection inside the burning shell will conspire with the formation of a giant structure. Moreover, numerical experiments show that, as soon as convective transport penetrates inside the main regions of the burning shell, the radius of the star will decrease. Figure 11 shows a numerical experiment in which the bottom of the adiabatic temperature is forced down into the burning shell itself. Note that these are static structures in which the gravothermal heat term ϵ_g is forced to zero throughout the star. We see that, as long as the adiabatic gradient stays far from the burning shell,

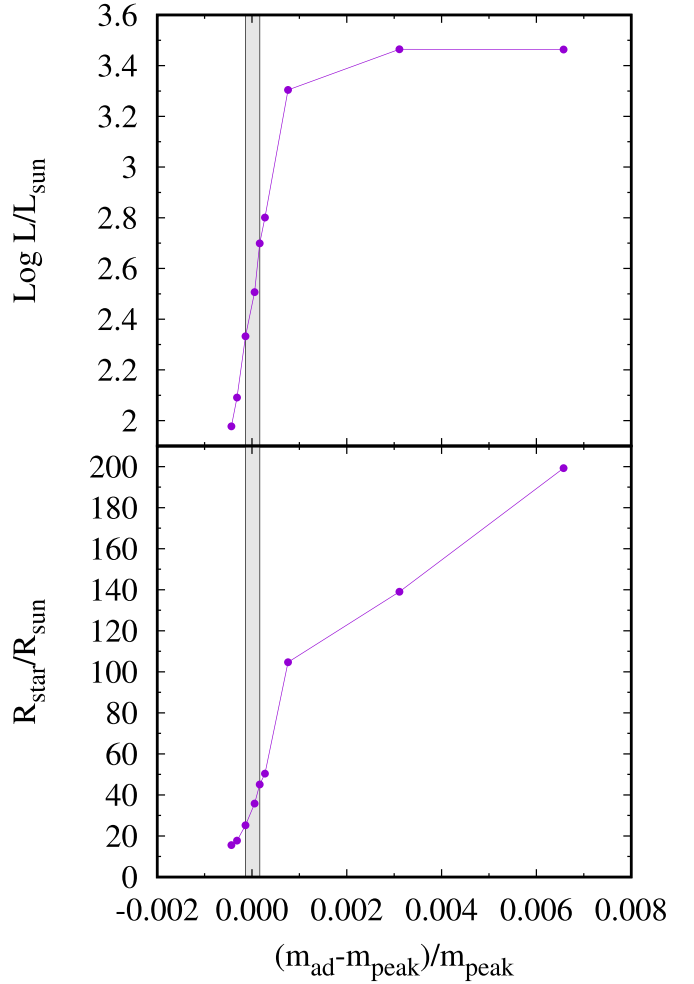


Figure 11. Impact of very deep convection on the luminosity and radius of the star.

the luminosity of the star remains unchanged because both the upper mantle and the burning shell can be considered radiative so the temperature of the burning shell and luminosity are determined by the equations derived in this paper. The radius of the star, on the other hand, is reduced as a consequence of the less steep density gradient imposed by adiabatic convection. However, as soon as convection reaches down to the burning shell itself luminosity is strongly affected, and the radius of the star drops suddenly. The more convection reaches into the burning shell, the smaller the final radius of the star. We find that, although relatively deep convection remains the main picture of the paper, as long as convection does not reach the bottom of the burning shell, stars with deep convective zones in the sense of this section (i.e., those in which convection reaches down to the burning shell itself) display much smaller radii.

Appendix D Envelope Integrations

Figures 12, 13, 14, and 15 show envelope integrations similar to those displayed by Figure 2 but for different conditions at the burning shell.

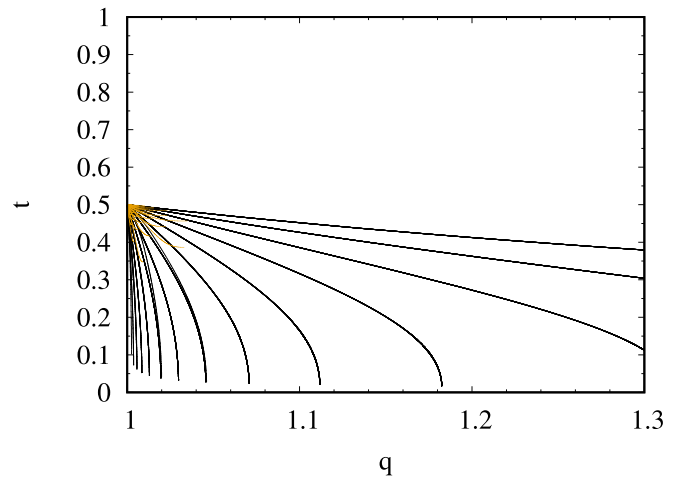
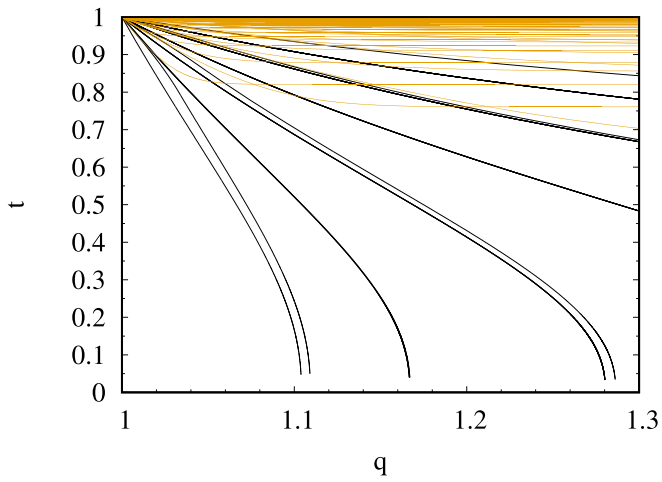
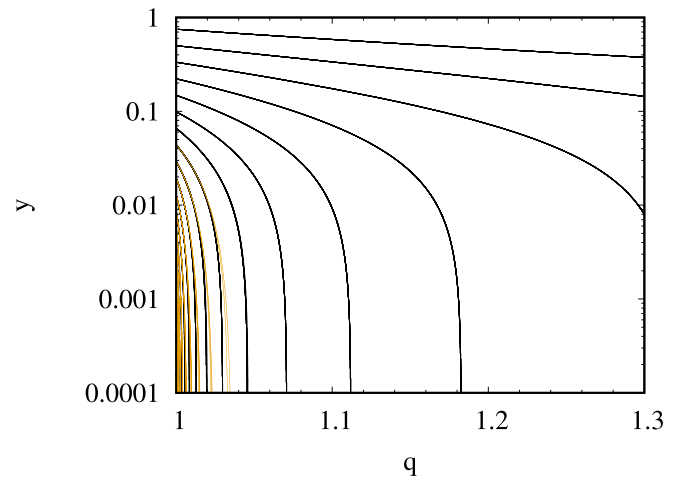
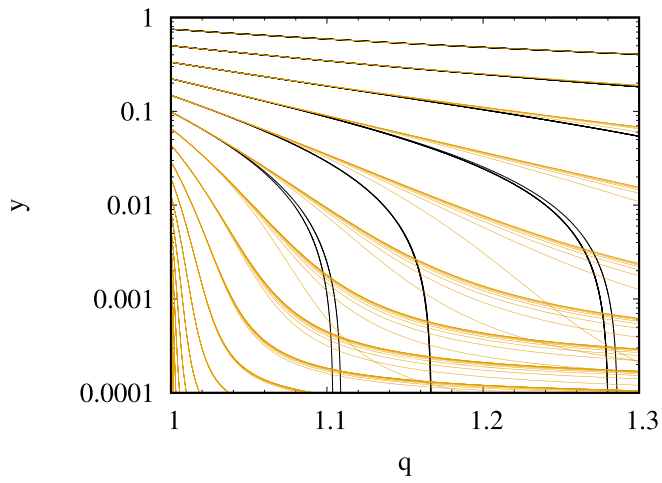
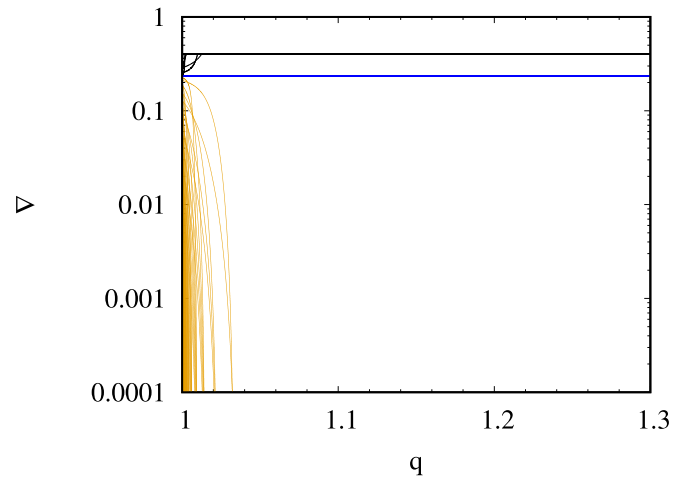
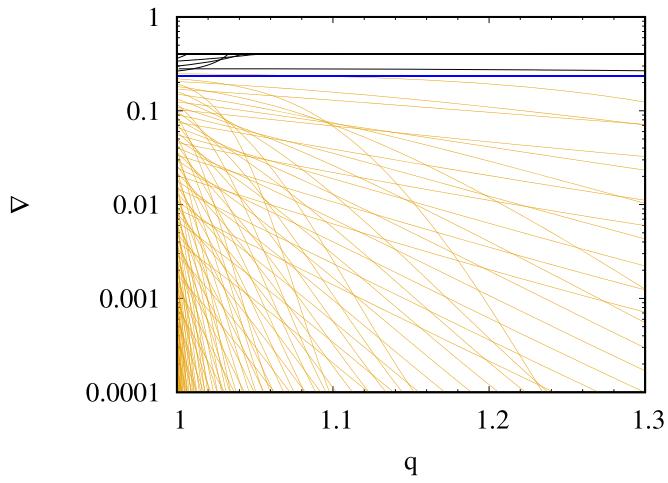


Figure 12. Envelope integration for different values of \mathbb{C} and y_+ , for $t_+ = 1$ and for a Kramers' opacity.

Figure 13. Envelope integration for different values of \mathbb{C} and y_+ , for $t_+ = 0.5$ and for a Kramers' opacity.

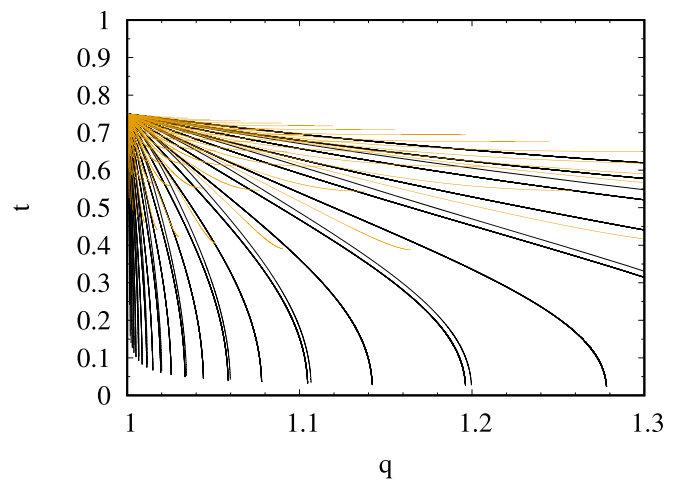
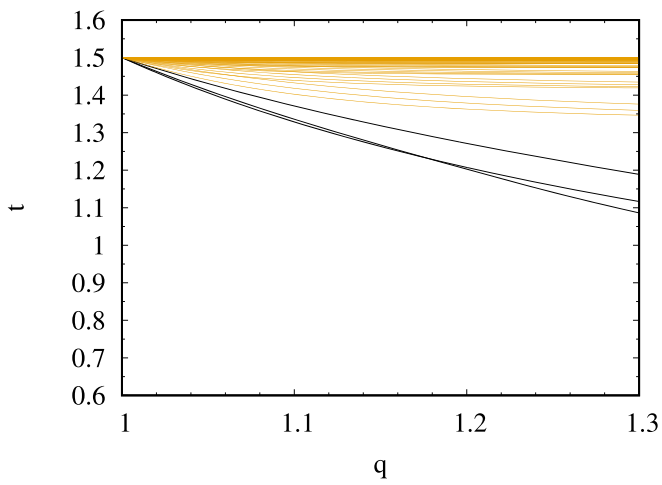
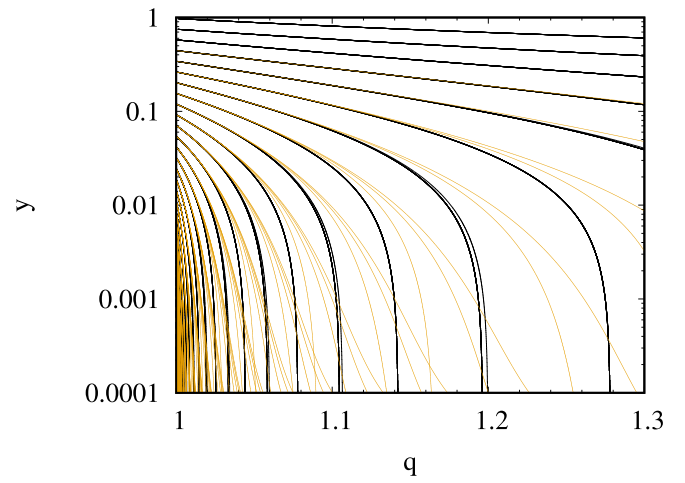
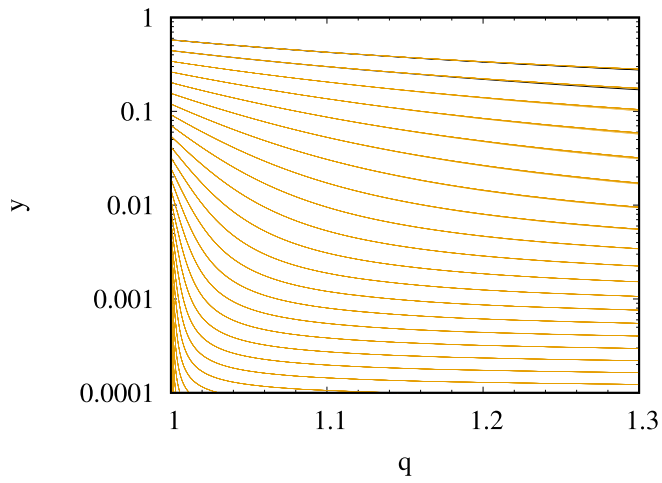
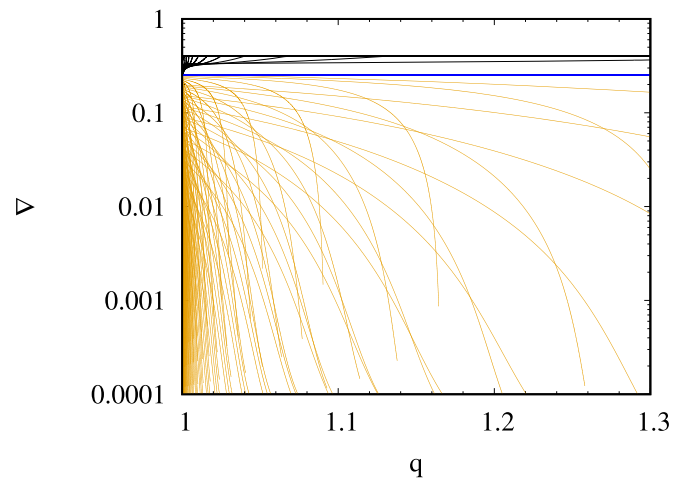
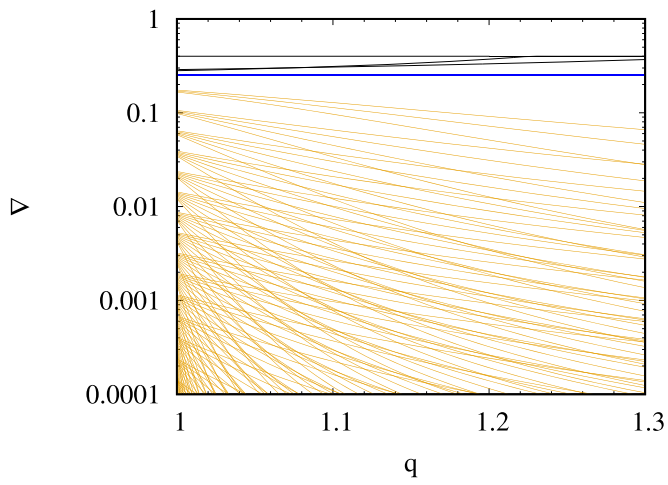


Figure 14. Envelope integration for different values of \mathbb{C} and y_+ , for $t_+ = 1.5$ and for a Kramer's opacity.

Figure 15. Envelope integration for different values of \mathbb{C} and y_+ , for $t_+ = 0.75$ and for a Thomson scattering-like opacity.

Appendix E

Early Evolution of the Burning Shell

As discussed in Section 2.3, when $\rho_+ \ll \rho_c$ and $P_+ \ll \bar{P}_c$ we can strictly demonstrate that $\Theta \simeq 1$, $\Pi \simeq 1$, $\zeta \simeq 1$, $T_0 \ll T_+$, and $R_s \ll R_0$ and all previous expressions are very simple. We show below that these approximations are still acceptable even on the very early stages of shell burning. From the hydrostatic equilibrium equation and using the definitions in Equation (5) we can see that the drop in pressure, temperature, and density immediately above the burning shell follows

$$\begin{aligned} \frac{dP}{P} \Big|_+ &\simeq -6 \left(\frac{T_c}{T_+} \right) \frac{R_s}{r^2} dr, \\ \frac{dT}{T} \Big|_+ &\simeq -6 \nabla_+ \left(\frac{T_c}{T_+} \right) \frac{R_s}{r^2} dr, \\ \frac{d\rho}{\rho} \Big|_+ &\simeq -6(1 - \nabla_+) \left(\frac{T_c}{T_+} \right) \frac{R_s}{r^2} dr. \end{aligned} \quad (\text{E1})$$

From Equation (18) we see that once the shell becomes active $F \simeq 2$ (Equation (15)) in the early stages of H-shell burning ($\nu \simeq 23$ at low temperatures of the CNO cycle), we have for $\nabla_+ \sim 0.25$ very roughly that $\rho_+ \sim \rho_-/2$ and $P_+ \sim P_-/2$. Using the very conservative approximation that at the lower boundary of the burning shell density and pressure are half their values at the core, we then have $\rho_+ \sim \rho_c/4$ and $P_+ \sim \bar{P}_c/4$ (in fact, in low-mass giants it will be much smaller than this due to the presence of a near isothermal inner mantle; see Section 3.1). From Equation (E1) and as long as $r \simeq R_s$ we can make the very rough approximation that $d\rho/\rho|_+ \simeq -18/4dr/r$ immediately above the burning shell. From the previous estimation we get that $\rho(r) \simeq \rho_+(r/R_s)^{-18/4}$. Integrating the upper mantle

$$\mathcal{Q}M_c = \int_{R_s}^{R_0} \rho(r) 4\pi r^2 dr, \quad (\text{E2})$$

where \mathcal{Q} is the fraction of the mass of the core we consider acceptable for $m(r) \simeq M_c$. Integrating out to $\mathcal{Q} = 0.2$ so that the approximation $m \simeq M_c$ is accurate to $\sim 20\%$, we get that $R_0 \simeq 1.4 R_s$, or the width of the upper mantle to be $\Delta R/R_s \simeq 0.4$. From this estimation we see that, already at the very early stages of H-shell burning the factor $(1 - R_s/R_0)$ in Equation (23) is a factor of 3 lower than 1 but not negligible. From this value of $\Delta R/R_s$ and the estimations of dP/P and dT/T at the upper boundary we get $T_0 \sim T_+ \exp(-6\nabla_+)(R_0/R_s) \sim 0.31T_+$ and $P_0 \sim \exp(-6)(R_0/R_s) \sim 0.0035P_+$. Then the factors Θ and Π in Equation (28) are both close to 1 even at this early stage and considering these conservative assumptions regarding the link between the values at the lower boundary (ρ_- , P_-) and their mean values at the core.

The importance of the estimations from the previous paragraphs cannot be downplayed as they tell us that already from the very early stages of H-shell burning the factors Π , Θ , and $(1 - R_0/R_s)$ in Equations (28) and (23) are of order 1, and consequently these equations are actual restrictions for the values of \bar{P}_c , T_c , and R_c . These restrictions play a key role in the increase in the density and pressure contrast ($\bar{\rho}_c/\rho_s$ and \bar{P}_c/P_s) between the shell and the core, so it is important to show that such relations are valid (even if only approximately) before the values of $\bar{\rho}_c/\rho_s$ and \bar{P}_c/P_s become huge. Once $\bar{\rho}_c/\rho_s$ and \bar{P}_c/P_s become large, the approximation $\Theta = 1$,

$\Pi = 1$ becomes very precise. It is then reasonable to assume for most practical estimations that $\Theta \simeq 1$, $\Pi \simeq 1$, $\zeta \simeq 1$, and $R_s \ll R_0$.

ORCID iDs

Marcelo M. Miller Bertolami  <https://orcid.org/0000-0001-8031-1957>

References

- Applegate, J. H. 1988, *ApJ*, **329**, 803
- Bhaskar, R., & Nigam, A. 1991, *ApJ*, **372**, 592
- Box, G. E. P. 1979, in *Robustness in Statistics*, ed. R. L. Launer & G. N. Wilkinson (Amsterdam: Academic Press), 201
- Cassisi, S., & Salaris, M. 2013, *Old Stellar Populations: How to Study the Fossil Record of Galaxy Formation* (Chichester: Wiley)
- Christensen-Dalsgaard, J. 2015, *MNRAS*, **453**, 666
- Eddington, A. S. 1926, *The Internal Constitution of the Stars* (Cambridge: Cambridge Univ. Press)
- Eggleton, P. P., & Cannon, R. C. 1991, *ApJ*, **383**, 757
- Eggleton, P. P., & Faulkner, J. 1981, in *Physical Processes in Red Giants*; Proc. of the Second Workshop, Astrophysics and Space Science Library, Vol. 88, ed. I. Iben & A. Renzini (Dordrecht: Reidel), 179
- Eggleton, P. P., Faulkner, J., & Cannon, R. C. 1998, *MNRAS*, **298**, 831
- Faulkner, J. 1997, *Stellar Ecology: Advances in Stellar Evolution* (Cambridge: Cambridge Univ. Press), 9
- Faulkner, J. 2005, in *Red Giants: Then and Now*, ed. D. Gough (Cambridge: Cambridge Univ. Press), 149
- Frost, C., & Lattanzio, J. C. 1992, *PASA*, **10**, 125
- Fujimoto, M. Y., & Iben, I. J. 1991, *ApJ*, **374**, 631
- Greggio, L., & Renzini, A. 2011, *Stellar Populations: A User Guide from Low to High Redshift* (Chichester: Wiley)
- Hansen, C. J., Kawaler, S. D., & Trimble, V. 2004, *Stellar Interiors: Physical Principles, Structure, and Evolution* (2nd ed.; New York: Springer)
- Hauptmann, H., Herrmann, F., & Schmidt, K. 2000, *AmJPh*, **68**, 421
- Hayashi, C. 1947, *PTPh*, **2**, 127
- Hayashi, C. 1949, *PhRv*, **75**, 1619
- Hekker, S., Angelou, G. C., Elsworth, Y., & Basu, S. 2020, *MNRAS*, **492**, 5940
- Höppner, W., & Weigert, A. 1973, *A&A*, **25**, 99
- Hoyle, F., & Lyttleton, R. A. 1949, *MNRAS*, **109**, 614
- Hoyle, F., & Schwarzschild, M. 1955, *ApJS*, **2**, 1
- Iben, I. J. 1993, *ApJ*, **415**, 767
- Iben, I. J., Jr. 2013, *Stellar Evolution Physics, Volume 2: Advanced Evolution of Single Stars* (Cambridge: Cambridge Univ. Press)
- Kippenhahn, R., Weigert, A., & Weiss, A. 2012, *Stellar Structure and Evolution* (Berlin: Springer)
- Lebreton, Y., Monteiro, M. J. P. F. G., Montalbán, J., et al. 2008, *Ap&SS*, **316**, 1
- MacDonald, J. 2015, *Structure and Evolution of Single Stars: An Introduction* (Bristol: IOP Publishing)
- Miller Bertolami, M. M. 2016, *A&A*, **588**, A25
- Öpik, E. 1938, *PTarO*, **30**, D1
- Prialnik, D. 2009, *An Introduction to the Theory of Stellar Structure and Evolution* (Cambridge: Cambridge Univ. Press)
- Renzini, A. 1984, in *IAU Symp. 105, Observational Tests of the Stellar Evolution Theory*, ed. A. Maeder & A. Renzini (Dordrecht: Reidel)
- Renzini, A., Greggio, L., Ritossa, C., & Ferrario, L. 1992, *ApJ*, **400**, 280
- Renzini, A., & Ritossa, C. 1994, *ApJ*, **433**, 293
- Salaris, M., & Cassisi, S. 2005, *Evolution of Stars and Stellar Populations* (Chichester: Wiley)
- Sandage, A. R., & Schwarzschild, M. 1952, *ApJ*, **116**, 463
- Schwarzschild, K. 1906, *Nachrichten von der Königlichen Gesellschaft der Wissenschaften zu Göttingen. Math.-phys. Klasse*, **195**, 41
- Silva Aguirre, V., Christensen-Dalsgaard, J., Cassisi, S., et al. 2020, *A&A*, **635**, A164
- Soker, N. 2008, *ApJL*, **674**, L49
- Stancliffe, R. J., Chieffi, A., Lattanzio, J. C., & Church, R. P. 2009, *PASA*, **26**, 203
- Sugimoto, D. 1997, *Stellar Ecology: Advances in Stellar Evolution* (Cambridge: Cambridge Univ. Press), 19
- Sugimoto, D., & Fujimoto, M. Y. 2000, *ApJ*, **538**, 837
- Weiss, A. 1983, *A&A*, **127**, 411
- Weiss, A. 1989, *A&A*, **209**, 135
- Whitworth, A. P. 1989, *MNRAS*, **236**, 505
- Yahil, A., & van den Horn, L. 1985, *ApJ*, **296**, 554